processes

MDPI

Article

Microfluidic Insights into the Effects of Reservoir and Operational Parameters on Foamy Oil Flow Dynamics during Cyclic Solvent Injection: Reservoir-on-the-Chip Aided Experimental and Numerical Studies

Ali Cheperli, Farshid Torabi * and Morteza Sabeti

Faculty of Engineering and Applied Science, University of Regina, Regina, SK S4S 0A2, Canada
* Correspondence: farshid.torabi@uregina.ca; Tel.: +1-306-585-5667

Abstract: This study examines the microfluidic characterization of foamy oil flow dynamics in heterogeneous porous media. A total of 12 microfluidic CSI experiments were conducted using reservoir-on-the-chip platforms. In addition, detailed PVT analysis was performed to characterise the heavy oil/solvent systems. Moreover, a numerical model constructed with CMG software package (2021.10) has been validated against the experimental findings in this study. A clear-cut visualization study provided by microfluidic systems revealed that factors including solvent type, pressure depletion rate, and reservoir parameters have a significant impact on foamy oil flow extension. It was found that a solvent containing a higher CO_2 content demonstrated more effective performance compared with other solvent compositions, owing to its capability to reduce viscosity, enhance swelling, and offer more gas molecules due to its superior solubility. Additionally, a high pressure-depletion rate amplifies the driving force for bubble nucleation, as well as reducing the amount of time available for bubble coalescence. In addition, lower reservoir porosity impedes bubble movement and delays coalescence, thus extending the foamy oil flow. Furthermore, with the aid of a robust image analysis technique, it was discovered that utilizing 100% CO_2 as a solvent resulted in a 17% increase in oil recovery over using 50% CO_2 and 50% CH_4. Furthermore, a 6% increase in oil recovery was achieved by applying a fast pressure depletion rate as opposed to a slow pressure depletion rate. Moreover, the numerical model constructed was found to be accurate in adjusting heavy oil recovery with an average relative error of 7.7%.

Keywords: cyclic solvent injection; foamy oil flow; microfluidic systems; solvent-based EOR

check for updates

Citation: Cheperli, A.; Torabi, F.; Sabeti, M. Microfluidic Insights into the Effects of Reservoir and Operational Parameters on Foamy Oil Flow Dynamics during Cyclic Solvent Injection: Reservoir-on-the-Chip Aided Experimental and Numerical Studies. *Processes* **2024**, *12*, 1305. https://doi.org/10.3390/pr12071305

Academic Editor: Syed Muhammad Shakil Hussain

Received: 26 April 2024
Revised: 17 June 2024
Accepted: 19 June 2024
Published: 24 June 2024

Copyright: © 2024 by the authors. Licensee MDPI, Basel, Switzerland. This article is an open access article distributed under the terms and conditions of the Creative Commons Attribution (CC BY) license (https://creativecommons.org/licenses/by/4.0/).

1. Introduction

Heavy oil reservoirs are typically exploited by using a combination of primary, secondary, and tertiary oil recovery techniques. Cold heavy oil production with sand (CHOPS) is one such method that harnesses natural reservoir energy to extract heavy oil while encouraging sand production. By stimulating the development of unconsolidated reservoir sand, this process increases oil recovery rates by enhancing porosity and permeability, aided by foamy oil flow dynamics. CHOPS typically achieves heavy oil production rates significantly higher than those projected by Darcy's law [1,2].

In secondary recovery methods like waterflooding and gas flooding, reservoir pressure is sustained, and crude oil displacement is facilitated by injecting water or gas. Waterflooding, for instance, is favoured due to its cost-effectiveness and simplicity. However, it yields lower oil recovery rates in heavy oil reservoirs because of displacement instability caused by unfavourable mobility ratios. Issues like viscous fingering, where injected water bypasses heavy oil, are common challenges in both waterflooding and gas flooding [3].

Thermal- and solvent-based methods serve as primary strategies for heavy oil recovery. In Situ combustion (ISC) [4,5], Steam-Assisted Gravity Drainage (SAGD) [6], Cyclic

Steam Stimulation (CSS) [7], and Steam Flooding (SF) are among the most commonly utilised thermal-based EOR techniques. ISC, pioneered during the 1940s and 1950s, faces uncertainties regarding its field-scale implementation [8]. CSS, however, has demonstrated commercial success in various field trials, though it is constrained by inadequate driving forces to propel heated fluids towards production wells [7,9]. SAGD, leveraging gravity drainage between horizontal wells, can achieve high oil flow rates [10] but is limited by reservoir characteristics and conditions such as thin pay-zones and bottom water [11–13].

Solvent-based methods offer an alternative approach to reducing heavy oil viscosity. Methods like Vapour-Assisted Petroleum Extraction (VAPEX), Cyclic Solvent Injection (CSI), and Solvent Flooding (SF) provide advantages in energy consumption, operational cost, improved oil quality, and environmental impacts over thermal-based techniques. They reduce energy consumption significantly compared to steam-based processes and require fewer surface facilities, leading to lower capital and operational costs. Additionally, proper solvent dissolution into heavy oil can enhance oil quality through in situ de-asphalting, while also offering environmental benefits by consuming less water and producing fewer greenhouse gases [14–16].

CSI, a technique for extracting heavy oil without using thermal methods, may represent a more environmentally friendly approach to exploiting heavy oil reservoirs. This method consists of three primary phases: injection, shut-in, and production. Initially, vapourised solvents such as CO_2, CH_4, C_3H_8, or their combinations are introduced into the heavy oil reservoir. Subsequently, the well is temporarily closed to allow the solvent to dissolve the crude oil, expand its volume, and drastically reduce its viscosity. Upon reopening the well, pressure depletion facilitates oil production [17].

Because of the elevated viscosity of heavy oil, when solvent exsolution transpires, the released solvent does not immediately convert into free gas. Instead, it remains dispersed within the oil as bubbles, a phenomenon known as foamy oil flow. This phenomenon significantly enhances heavy oil production, especially in methods like cold heavy oil production with sand (CHOPS) and CSI [18,19]. Smith conducted pioneering analyses of foamy oil's distinct production behaviour, attributing its complexity to the intricate interaction between heavy oil and gas bubbles. This behaviour, characterised by unexpected mobilities, challenges traditional assumptions regarding oil mobility [1].

Numerous investigations have been undertaken to evaluate the effectiveness of the CSI technique across various reservoir and operational conditions. Qazvini Firouz and Torabi performed experimental studies to evaluate the impact of pressure, soaking time, and solvent type on the huff-and-puff process. They concluded that utilizing CO_2 under near-supercritical characteristics achieved the most improved oil recovery rate. Longer soaking times at low operating pressures did not significantly improve final oil recovery [20]. Alshmakhy and Maini assessed the effectiveness of cyclic CO_2 injection for increasing heavy oil recovery from depleted reservoirs, achieving the most amount of incremental oil production with a recovery of 8.39% [21]. Jia et al. proposed a modified CSI method called pressure pulsating CSI. Their technique involves a pressure control strategy throughout the production phase: initially, the pressure is decreased to initiate foamy oil flow; next, the pressure is raised back to a certain value; finally, a specific pressure gradient across the injector and producer is maintained for gas flooding. This sequence of steps makes one pressure pulse and can be conducted repeatedly multiple times over the production phase. According to their findings, pressure pulsating CSI processes demonstrated significantly higher oil recovery factors and production rates than traditional CSI [22]. Du et al. examined the viability of CSI as a post-CHOPS method, finding that wormholes improve CSI performance, especially when located at the reservoir bottom. Additionally, using a power function regression, they established a relationship between oil production rate and drainage height independent of model length and diameter [23].

A compositional simulator was used by Ravel and Anterion to replicate CO_2 huff-and-puff in order to gather preliminary data on oil production. Their simulations included factors such as oil swelling, gravity drainage, and capillary imbibition, as well as an in-

terfacial film method to describe mass transfer [24]. Ivory et al. performed a primary oil production experiment prior to CSI. In addition, they conducted simulation study and a robust production history match procedure. To account for the delay in reaching equilibrium concentration during solvent exsolution or dissolution into oil, a non-equilibrium solvent exsolution/dissolution was incorporated into the model. There was a significant influence of factors such as the reaction rate, solvent mass transfer coefficient, oil density, solubility, and relative permeability on solvent injectivity [25]. Based on a study conducted by Chang and Ivory, the simulation study was expanded from lab-to-field scales. Different wormhole models were considered to replicate post-CHOPS reservoir behaviour, emphasizing the need to consider non-equilibrium phase behaviour [26]. CSI was evaluated from both a technical and an economic perspective by Shokri and Babadagli. They found that although heavier solvents resulted in higher heavy oil recovery factors, lighter solvents were considered to be more economically viable [27].

Prior studies have mostly focused on analysing the volumetric expansion and overall stability aspects of foamy oil flow. However, for comprehending the foamy oil flow, it is necessary to examine its dynamics. Foamy oil flow includes bubble evolution, which consists of different stages of nucleation, growth, and coalescence. Using advanced microfluidic setups that provide precise visualization capabilities, this project examined the intricate impact of reservoir characteristics and operational variables on foamy oil flow dynamics. Additionally, it employed meticulous data acquisition methodologies in conjunction with robust image analysis techniques to evaluate the overall effectiveness of the CSI process across a variety of reservoir and operational settings. In addition, detailed PVT analysis was performed to assess the characteristics of the heavy oil/solvent systems employed in this project. Moreover, a numerical model constructed with the CMG software package (2021.10) has been validated by taking into account the experimental findings in this study. Identifying the complex interactions between these parameters will contribute to a greater understanding of foamy oil flow behaviour, and therefore to the overall performance of CSI.

2. Materials and Methods

2.1. Heavy Oil Properties

Using kerosene in a certain amount, a heavy oil sample from Plover Lake in Canada with an initial viscosity of more than 100,000 cP was diluted to achieve a viscosity of 1600 cP at 21 °C. To measure the viscosity of the heavy oil, a Brookfield Viscometer (Brookfield Engineering Laboratory, INC., Middleborough, MA, USA) was used to continuously mix and measure the viscosity of the diluted heavy oil until the desired viscosity has been achieved. Moreover, a gas chromatography analysis of the prepared sample was conducted. The physical characteristics of the diluted heavy oil sample such as density, molecular weight, and viscosity are provided in Table 1.

Table 1. Properties of the diluted heavy oil sample.

Molecular Weight (g/mol)	Density (g/cm^3)	Viscosity (cP at 21 °C)
374	0.974	1600

2.2. Heavy Oil/Solvent System Properties

A schematic illustrating the applied setup for preparing the heavy oil/solvent systems is shown in Figure 1. This experimental setup includes a gas solvent supply cylinder, two transfer cylinders (Cylinder 1 and Cylinder 2), two ISCO pumps (with a capacity of 500 mL) (Teledyne ISCO INC, Lincoln, NE, USA), five pressure gauge tools, six valves, and the required connections. Using this setup, three heavy oil/solvent systems were prepared by mixing the diluted heavy oil sample with specific solvents (CO_2 and mixtures of CO_2/CH_4) at a certain saturation pressure and temperature.

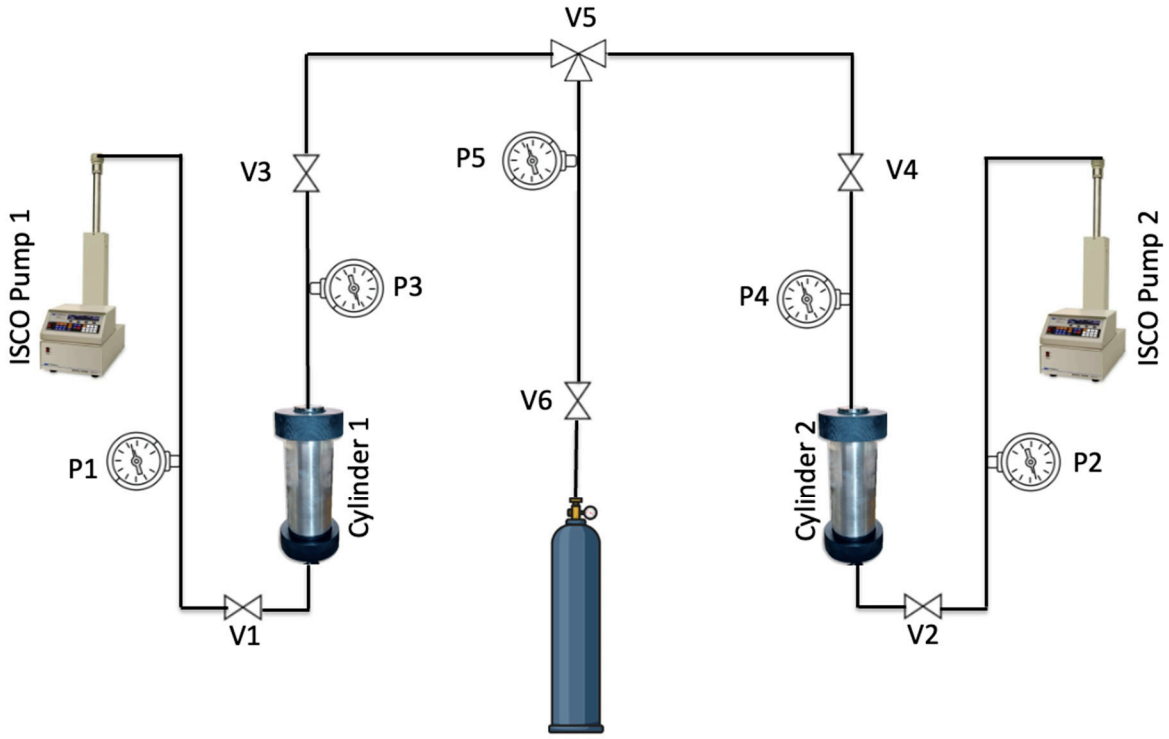

Figure 1. Heavy oil/solvent preparation setup.

Cylinder 1 was initially filled with predetermined amount of heavy oil to initiate the process. Following this, gas was injected from the top to facilitate contact between the heavy oil and the solvent, resulting in their mixing and subsequent dissolving. Gas injection was carried out at a pressure exceeding 3600 kPa to facilitate the preparation of heavy oil/solvent systems at the desired saturation pressure, which was set at 3600 kPa. A pressure of 3600 kPa was applied to the bottom of the piston in Cylinder 1, and this pressure was maintained even as the gas dissolved and the pressure in the system decreased. A two-day period was then allowed for the mixture to thoroughly mix in Cylinder 1.

Cylinders 1 and 2 were then gradually connected with a valve which allowed fluid from Cylinder 1 to enter Cylinder 2. The pressure of Pump 2 was set at 3600 kPa, while the pressure of Pump 1 was set slightly above 3600 kPa in order to facilitate the transfer of fluid between these two cylinders. It was thus possible to maintain the fluid pressure above 3600 kPa throughout the transfer process. During this process, fluid pressure was monitored by pressure gauges connected to the input and output of both cylinders. After the transfer was completed, the valve between the two cylinders was closed and the fluid was given an additional two days to mix and dissolve. The fluid was then recycled back into Cylinder 1. It was necessary to repeat the fluid transformation between the two cylinders several times to generate heavy oil/solvent systems. Similarly, in order to prepare the other heavy oil/solvent systems, the procedure was repeated with the two other gas sources, each of which had a different composition of gas.

2.2.1. Constant Composition Expansion (CCE) Tests

Figure 2 shows the setup used for the Constant Composition Expansion (CCE) test. This setup consists of a glass cylinder, a back pressure regulator, an ISCO pump (Teledyne ISCO INC, Lincoln, NE, USA), and the necessary connections. The objective of this experiment was to examine the properties of three different heavy oil/solvent systems. A certain quantity of the heavy oil/solvent sample was introduced from the bottom of the glass cylinder at a pressure exceeding 3600 kPa. The thin hydraulic oil located above the piston within the cylinder, which is manipulated using the pump, controls the pressure and volume of the fluid contained within the glass cylinder. In the following stages, the

fluid pressure was gradually reduced, allowing the oil and gas to reach equilibrium at each stage. Upon achieving equilibrium, the volume of gas and liquid, along with the pressure of the system, were recorded.

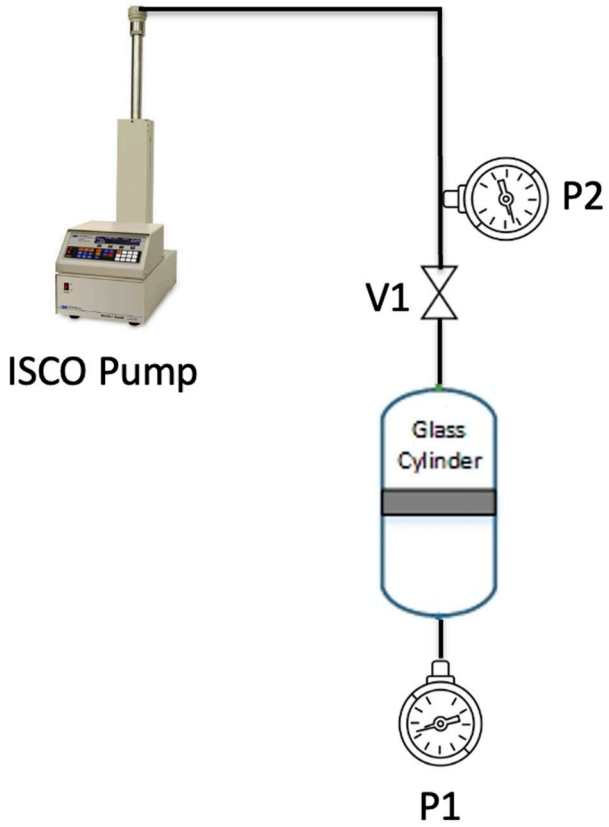

Figure 2. Constant Composition Expansion test setup.

2.2.2. Differential Liberation (DL) Tests

Differential liberation (DL) test was performed for the prepared heavy oil/solvent systems using setup shown in Figure 3. Our laboratory designed a comprehensive set-up that consisted of a glassy cylinder, capillary viscometer, online density measurement instrument, gas bubbler for measuring the volume of gas released from the oil, compact liquid trapper, digital gas flow meter, ISCO pump sets, back pressure regulator, nitrogen gas cylinder, and all the necessary connections. Designed to facilitate two-phase tests, this system also measures the properties of the liquid phase within the operational oil system at the same time.

Initially, a certain amount of the prepared heavy oil/solvent systems was introduced into the glass cylinder at a pressure exceeding 3600 kPa. Through the ISCO pump (Teledyne ISCO INC, Lincoln, NE, USA), the heavy oil/solvent system pressure was manipulated, by allowing the piston to move downward inside the cylinder. As a result of this movement, the fluid pressure decreased and the volume of the system increased. Four distinct stages of pressure reduction were used to gradually reduce the system's pressure and measure the properties at these different pressure stages. With each decrease in pressure, a certain quantity of gas was evolved from the liquid. A sufficient amount of time was allowed for the gas and liquid phases of the system to reach equilibrium at each stage. In order to infer equilibrium, it was observed that there were no macroscopic changes at the interface between the oil and gas phases. This was followed by the recording of the oil and gas levels, and the evolved gas was slowly expelled from the top of the cylinder. In order to control the output fluid pressure, a back pressure regulator (BPR) was positioned immediately prior to the liquid trap.

The expelled gas passed through the capillary viscometer, online densitometer, and liquid trap before being directed towards a gas bubbler. Gas properties were calculated by using the pressure and volume of the released gas measured in the gas bubbler. As the gas was evacuated from the cylinder, a small amount of oil was also discharged towards the capillary viscometer and density meter. In this way, the viscosity and density of oil at specific pressures could be measured.

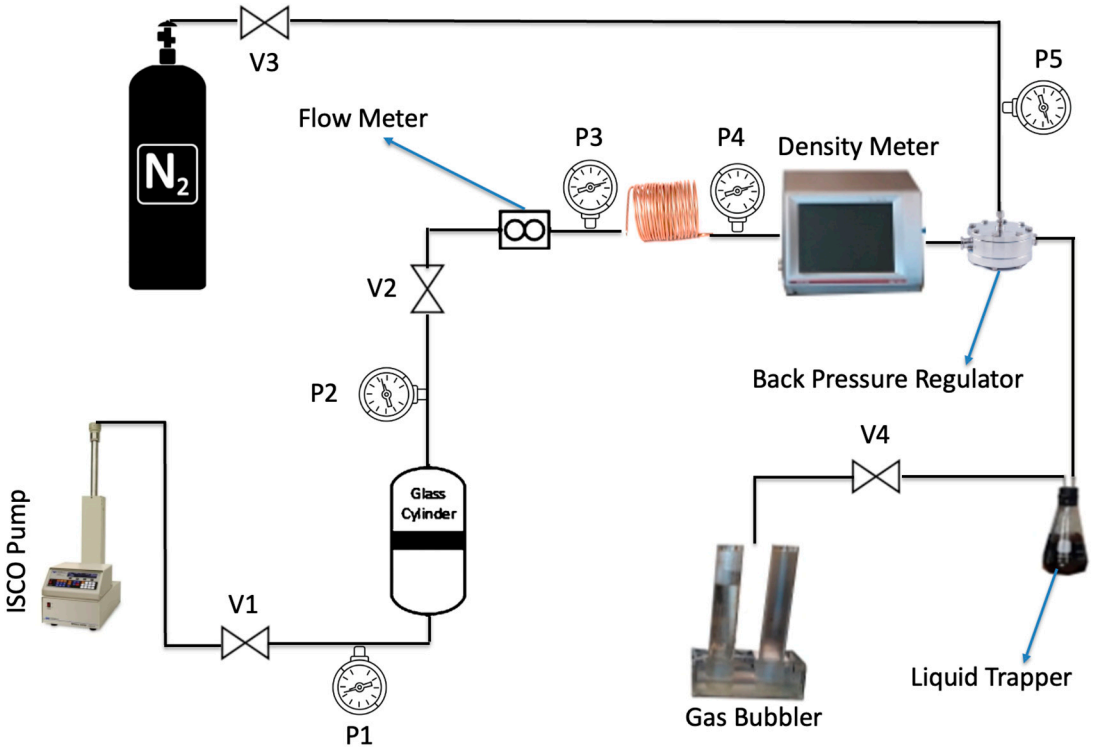

Figure 3. Differential liberation test setup.

2.3. Microfluidic Experiments

Equipped with the state-of-the-art computer-controlled laser machine along with high-temperature furnace, our research lab is capable of extensively designing and manufacturing various types of microfluidic systems for microscopic investigation of heavy oil recovery processes. Microfluidic systems enable the visualization study of the underlying mechanisms, the solvent–oil interface locating, foamy oil generation, foamy oil stability, and saturation distributions throughout the model. Two microfluidic systems have been constructed as part of this project. Described below is the procedure for manufacturing and measuring the properties of the microfluidic systems.

2.3.1. Construction of the Microfluidic Systems

Heterogeneous porous media structures, possessing desired lengths and widths, were designed using AutoCAD software (2024), a powerful engineering tool well known for its precision. A random arrangement of grains was used to design the heterogeneous pore structures in AutoCAD (2024). The objective of the design process was to achieve a specific porosity level, which was initially determined using image analysis. Following the design phase, the digital model was transferred to the computer connected to the laser machine, which translates the design onto a glass surface. A second identical piece of glass was prepared after the design was etched onto the glass. Both glass substrates were carefully assembled and placed in a high-temperature furnace. A controlled environment in the furnace allowed the two glass substrates to fuse together seamlessly. Upon completion of this fusion process, a robust microfluidic system was created, ready for further investigation and analysis. Regarding the experimental measurement of the porosity, through the use

of a vacuum pump, the microfluidic systems were vacuumed. Following this, water was injected into the models to facilitate the measurement of pore volume and, consequently, the determination of porosity [28]. The porosities for microfluidic system 1 and microfluidic system 2 are 47% and 32%, respectively. These values were also obtained through counting the pixels of grains and pore spaces with the aid of image analysis. Additionally, in order to measure the absolute permeability, an injection of water at distinct, predetermined flow rates was carried out, followed by meticulous recording of the pressure differential between the injection point and the production point. At the production end, adequate time was provided for the flow to stabilise. By using the Darcy equation, permeability was determined at each flow rate [28]. Several iterations of this process were performed, resulting in average permeability values of 5.6 Darcy and 8.7 Darcy for microfluidic system 1 and microfluidic system 2, respectively. Additionally, the average grain diameter is 2.6 mm in microfluidic system 1 and 4.7 mm in microfluidic system 2.

2.3.2. CSI Experiment Using Microfluidic System

As part of this study, a total of 12 microfluidic CSI tests were meticulously conducted, each of which served as an exploration into the intricacies of the foamy oil flow behaviour and overall performance of the CSI process. Two distinct micromodel configurations were examined in these tests, providing a pore-scale view of fluid dynamics in porous media. Additionally, the experimental design differentiated between rapid pressure depletion at 12 kPa/min and slower depletion at 6 kPa/min, enabling a thorough analysis of system responses under different pressure regimes. Through conducting multiple CSI tests, the aim was to evaluate the efficiency of CSI strategies under a variety of conditions. Furthermore, the use of two micromodel setups added depth to the analysis, allowing microscopic examination of fluid flow patterns and saturation distributions. Additionally, three different heavy/oil solvent systems were explored, each with distinct compositional characteristics. In addition to providing a deeper understanding of fluid behaviour within porous media, this approach provided insights into the interaction between operational parameters and reservoir heterogeneity. Details of each test are depicted in Table 2. In order to conduct the comprehensive microfluidic CSI tests described above, meticulous attention was paid to the execution of the production phase of a single cycle. Figure 4 illustrates the well-designed experimental setup, which encompasses a series of specific steps for precise data analysis.

Table 2. CSI scenarios.

Test No.	Porosity	Depletion Rate (kPa/min)	Solvent Type
Test 1	47%	12	100% CO_2
Test 2	47%	12	75% CO_2 and 25% CH_4
Test 3	47%	12	50% CO_2 and 50% CH_4
Test 4	32%	12	100% CO_2
Test 5	32%	12	75% CO_2 and 25% CH_4
Test 6	32%	12	50% CO_2 and 50% CH_4
Test 7	47%	6	100% CO_2
Test 8	47%	6	75% CO_2 and 25% CH_4
Test 9	47%	6	50% CO_2 and 50% CH_4
Test 10	32%	6	100% CO_2
Test 11	32%	6	75% CO_2 and 25% CH_4
Test 12	32%	6	50% CO_2 and 50% CH_4

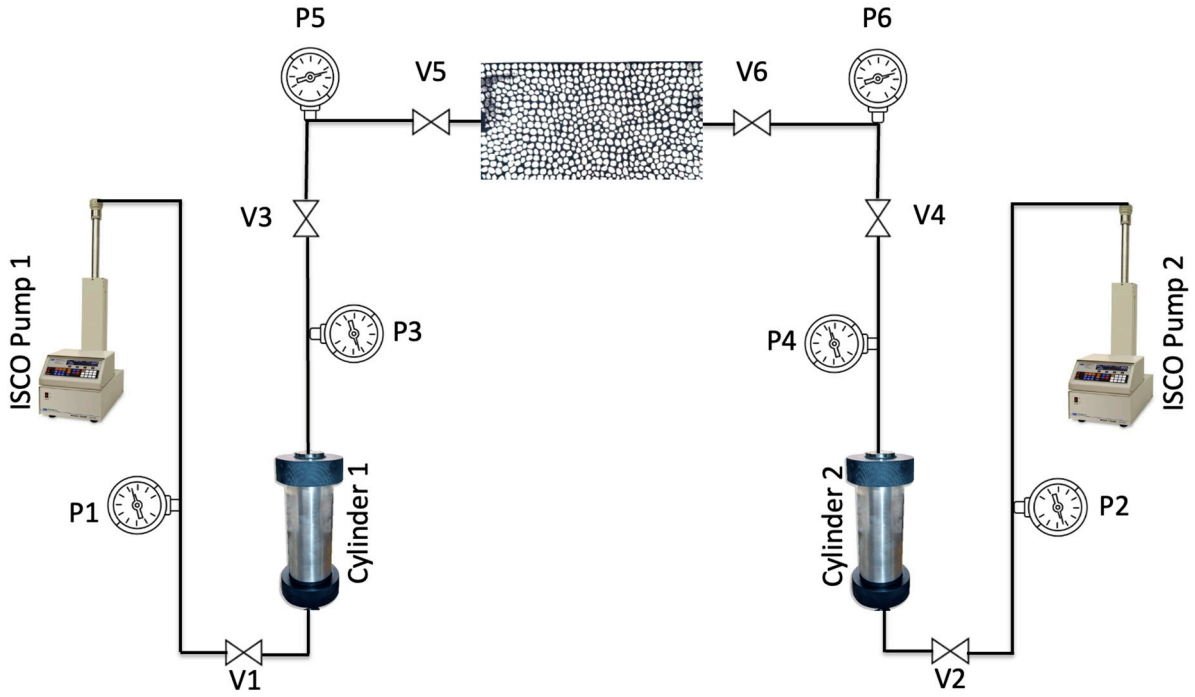

Figure 4. Experimental setup for microfluidic CSI tests.

In the initial phase, the system pressure was gradually increased up to 1500 kilopascals (kPa). This elevation in pressure was carefully executed, beginning with the controlled introduction of gas from Cylinder 1 into the micromodel, facilitated by Pump #1. The gas injection continued until the micromodel pressure seamlessly reached the desired 1500 kPa threshold. Following the establishment of the necessary pressure, heavy oil/solvent, which is held within Cylinder 2 at 1500 kPa, was introduced into the micromodel. This operation, which was precisely controlled by Pump #2, maintained a constant flow rate of 0.1 millilitres per minute (mL/min). The measured and consistent flow ensured optimal saturation of the micromodel, which is crucial to the accuracy of the test. Once saturation was confirmed, both valve #5 (V5) and valve #6 (V6) were closed, Pump #2 was stopped, and the transition to production was initiated. This phase was conducted by systematically reducing the system pressure using Cylinder #1 in conjunction with Pump #1 and opening valve #5 (V5).

Throughout the testing process, a comprehensive array of qualitative and quantitative data was collected. As part of this process, numerous pictures and videos were meticulously documented at strategic intervals. These visual records served as invaluable assets for subsequent image analysis, facilitating both qualitative and quantitative assessments of experimental outcomes. Essentially, the rigorous execution of the aforementioned steps, complemented by meticulous attention to detail and precision, enabled the evaluation of the CSI process to acquire robust data.

2.4. Data Measurement Techniques

In this study, images captured during CSI tests within microfluidic systems were analysed quantitatively using the k-cluster mean approach through MATLAB (2020a). Using this technique, distinct sections within the images are segmented and quantified to provide valuable insights into fluid dynamics and heavy oil recovery.

Prior to conducting image analysis, pre-processing steps were carried out in order to enhance the clarity of the image and reduce noise. The quality of the captured images may be improved by operations such as denoising, contrast enhancement, and edge detection. A key element of the data measurement technique is the segmentation of images using the k-cluster mean algorithm. The algorithm partitions the image into k clusters based on the intensity of pixels and the spatial distribution of pixels. In selecting k, consideration

should be given to the number of distinct sections that will be identified within the image. Due to the nature of the images, three distinct segments, including the heavy oil phase, porous media grain section, and dispersed bubble section, are considered. Using the pixel counts associated with each segment, the segmented sections are quantified. At specific time intervals, this provides a measure of the relative area occupied by each phase within the microfluidic system. A key application of the quantitative data derived from image analysis is the estimation of heavy oil recovery. The technique enables the calculation of heavy oil recovery rates by assuming a direct relationship between the area of the dispersed bubbles and the amount of oil extracted from the system. This image analysis technique also helps to extract detailed information regarding the nucleation, growth, and coalescence of bubbles, as well as the efficiency of the CSI process in terms of heavy oil recovery.

In discussing the calibration process for image analysis within this project, it is crucial to highlight the meticulous approach undertaken. Among the most important aspects of ensuring accuracy is the calibration of thresholds that are used to distinguish between segments. An important aspect of this calibration process involves the direct measurement of porosity within each microfluidic system. The algorithm calculates the area occupied by grains within the porous media and confirms the number of pixels that correspond to grains by using the porosity values. The purpose of this process is to improve the accuracy of the analysis by ensuring that calculated values are in accordance with experimental results. Additionally, the calibration process includes a comprehensive visual analysis of the segmented regions identified by the algorithm. As a further validation layer, visual inspection allows quantitative and qualitative findings to be corroborated.

2.5. Numerical Modelling

In order to perform parameter regression, the heavy oil/solvent system properties obtained from CCE and DL tests were input into CMG WINPROP (2021.10). A history match was performed for each of the three heavy oil/solvent systems in the PVT simulator. In addition to dead oil properties, there was a total of 12 sets of properties that were input for the history match.

In order to ensure accuracy and reliability in its predictions, CMG WINPROP (2021.10) uses a sophisticated approach to fluid characterization, integrating multiple robust methodologies. Peng–Robinson Equation of State (PR-EOS), as described via Equations (1)–(7), is a fundamental thermodynamic tool used to describe fluid behaviour under various conditions [29,30].

$$P = \frac{RT}{V-b} - \frac{a(T)}{V(v+b)+b(v-b)} \tag{1}$$

where

$$a(T) = a(T_c)\alpha(T_r,\, \omega) \tag{2}$$

$$b = b(T_c) \tag{3}$$

$$a(T_c) = 0.45724\frac{R^2T_c^2}{P_c} \tag{4}$$

$$b(T_c) = 0.07780\frac{RT_c}{P_c} \tag{5}$$

$$\alpha(T_r,\, \omega) = \left[1 + \left(0.37464 + 1.54226\omega - 0.26992\omega^2\left(1 - \sqrt{T_r}\right)\right)\right]^2 \tag{6}$$

$$T_r = \frac{T}{T_c} \tag{7}$$

where P represents the system's pressure in kilopascals, T denotes temperature in Kelvin, R signifies the universal gas constant in cubic metres per kilopascal per kilomole per Kelvin, P_c stands for critical pressure in kilopascals, T_c denotes critical temperature in Kelvin, T_r represents reduced temperature in Kelvin, V stands for molar volume in cubic centimetres per mole, and ω indicates the acentric factor.

In addition, Twu [31] and Lee and Kesler [32] correlations were utilised to establish the initial parameters. Using these correlations, it is possible to estimate properties such as the T_c, P_c, and ω of the dead oil component that can be used in PR-EOS. A fluid model can be fine-tuned based on the precision of these initial estimates. In addition, the Pedersen Corresponding State Model, which is renowned for its ability to predict fluid properties, has been applied in order to predict liquid viscosity [33]. The purpose of this step is to ensure a harmonious match between the simulated results and empirical data obtained from comprehensive CCE and DL tests. A tuned fluid model achieves a heightened level of accuracy by incorporating experimental measurements into the predictive framework. This allows the model to capture the intricate behaviour of the fluid dynamics that exist in the solvent/heavy oil systems. The fluid model, once calibrated, serves as the foundation for numerical simulations of the CSI process. These simulations rely on the equilibrium K values computed from the tuned PR-EOS model, which are derived through Equation (8) proposed by Ivory et al. [25,34]:

$$K = \left(\frac{kv_1}{P} + kv_2 P + kv_3\right) e^{\frac{kv_4}{T - kv_5}} \tag{8}$$

where, P is pressure (kPa), T stands for temperature (K), and kv_1, kv_2, kv_3, kv_4, and kv_5 denote the coefficients corresponding to the particular solvent component.

Moreover, CMG STARS (2021.10) was utilised to construct a simulation model capable of replicating the CSI tests. Cartesian meshes consist of $15 \times 5 \times 1$ grids, each measuring 15 cm long, 5 cm wide, and 1 mm thick were considered. In addition, a four-component model including dead oil, solution gas, dispersed gas, and free gas have been considered in this model. In order to simulate pressure depletion, a production well was defined to gradually reduce bottom-hole pressure from 1500 kPa to atmospheric pressure.

In order to include the foamy oil flow behaviour in the simulation, in this project, the non-equilibrium exsolution process has been considered. In this process, two types of pseudo-chemical reactions are considered. The first reaction describes the dynamics of bubble nucleation and growth. As a matter of fact, it depicts the rate of the change of dissolved gas into dispersed gas. Equation (9) shows this process [34]:

$$Solvent\ (liquid) \rightarrow Solvent\ (Dispersed\ Gas) \tag{9}$$

Moreover, the reaction rate equation is as follows:

$$R_1 = R_{rk1} e^{-\frac{E_{ak2}}{RT}} \prod C_j^{N_j} \tag{10}$$

The second reaction depicts the dynamics of bubble coalescence. As a matter of fact, it shows the rate of the change of dispersed gas into free gas. Equation (11) demonstrates this process:

$$Solvent\ (Dispersed\ gas) \rightarrow Solvent\ (free\ gas) \tag{11}$$

The related reaction rate equation for the above reaction is as shown in Equation (12).

$$R_2 = R_{rk2} e^{-\frac{E_{ak2}}{RT}} \prod C_j^{N_j} \tag{12}$$

By considering an isothermal condition, the value of E_{ak} can be considered as zero. Therefore, the only unknown parameters in Equations (10) and (12) are R_{rk1} and R_{rk2}, respectively. As for the simulator calibration, with the aid of CMG CMOST (2021.10), gas–oil relative permeability, diffusion coefficients, and kinetic model parameters (R_{rk1} and R_{rk2}) were adjusted to align with the experimental findings.

It is important to note that in this project, foamy oil is expected to have a viscosity similar to heavy oil/solvent systems at various pressures. Furthermore, mixtures of CO_2

and CH_4 are combined and treated as one solvent when specifying the solvent for each scenario. Moreover, all scenarios were assumed to have consistent permeability curves.

3. Results and Discussion

This section provides the results of the comprehensive analysis of the PVT data, illustrating how various parameters influence the heavy oil swelling factor and viscosity reduction. The findings of the microfluidic examination coupled with detailed image analysis reveal the intricate relationship between these parameters and their influence on the efficiency of the CSI process. In addition, a detailed description of the results of the numerical simulations conducted to model the CSI process is presented in this section.

3.1. The properties of the Heavy Oil/Solvent Systems

Regarding the experimental findings concerning the PVT analysis, Table 3 provides comprehensive insights into the characteristics of the heavy oil/solvent systems. Among these characteristics are the mole percent of gas, the density, the viscosity, and the swelling factor at four different pressures using 100% CO_2 as the solvent.

Table 3. PVT data for heavy oil/solvent system 1, where the solvent is 100% CO_2.

Pressure (kPa)	Gas Mole Fraction (%)	Oil Density (Kg/m^3)	Oil Viscosity (cP)	Swelling Factor (m^3/m^3)
400	6.2	967	1253	1.01
1415	20.6	946	770	1.03
2625	35.7	918	416	1.07
3600	46.8	890	241	1.11

An examination of the table in detail reveals noteworthy trends. A notable elevation in the swelling factor is observed at 3600 kPa, emphasizing the potent influence of CO_2. Moreover, the oil viscosity is decreased significantly, demonstrating the effectiveness of CO_2 in enhancing swelling and mitigating viscosity at the same time.

Accordingly, Table 4 illustrates analogous PVT properties in the presence of a solvent containing 75% CO_2 and 25% CH_4.

Table 4. PVT data for heavy oil/solvent system 2, where the solvent is 75% CO_2 and 25% CH_4.

Pressure (kPa)	Gas Mole Fraction (%)	Oil Density (Kg/m^3)	Oil Viscosity (cP)	Swelling Factor (m^3/m^3)
400	6.2	965	1253	1.01
1415	16.5	952	890	1.02
2625	24.4	940	665	1.04
3600	28.0	904	577	1.05

Based on a comparison of Tables 3 and 4, it can be seen that the swelling factor in heavy oil/solvent system 1 has been reduced compared to heavy oil/solvent system 2. This results in a smaller reduction in oil viscosity than in the former case, which suggests a relatively poor reduction in viscosity and swelling caused by the presence of CH_4.

Table 5 provides information regarding the PVT data for a third scenario featuring a solvent composition of 50% CO_2 and 50% CH_4.

Table 5. PVT data for heavy oil/solvent system 3, where the solvent is 50% CO_2 and 50% CH_4.

Pressure (kPa)	Gas Mole Fraction (%)	Oil Density (Kg/m^3)	Oil Viscosity (cP)	Swelling Factor (m^3/m^3)
400	5.2	966	1290	1.00
1415	13.3	956	994	1.01
2625	18.5	948	829	1.02
3600	21.4	943	746	1.03

Accordingly, both the viscosity and the swelling factor differ from the previous cases. The presence of CH_4 in the solvent mixture has significantly reduced the solvent's ability to reduce viscosity. A substantial decrease in swelling factor is also observed in the data.

Therefore, these tables provide a comprehensive analysis of how CO_2 affects viscosity and swelling factor, two crucial parameters that play a critical role in the overall efficiency of the CSI process.

3.2. Microfluidic Tests Results

As mentioned in Section 2, a total of 12 microfluidic tests have been conducted to assess the effect of different factors on foamy oil flow behaviour and heavy oil recovery. In this project, images captured during CSI tests within microfluidic systems were analysed quantitatively using the k-cluster mean approach through MATLAB (2020a). Prior to conducting image analysis, pre-processing steps were carried out in order to enhance the clarity of the images and reduce noise. The quality of the captured images may be improved by operations such as denoising, contrast enhancement, and edge detection. A key element of the data measurement technique is the segmentation of images using the k-cluster mean algorithm. The algorithm partitions the image into k clusters based on the intensity of pixels and the spatial distribution of pixels. In selecting k, consideration should be given to the number of distinct sections that will be identified within the image. Due to the nature of the images, three distinct segments, including the heavy oil phase, porous media grain section, and dispersed bubble section, were considered. Using the pixel counts associated with each segment, the segmented sections are quantified. At specific time intervals, this provides a measure of the relative area occupied by each phase within the microfluidic system.

A key application of quantitative data derived from image analysis was the estimation of heavy oil recovery. The technique enables the calculation of heavy oil recovery values by assuming a direct relationship between the area of the dispersed bubbles and the amount of oil extracted from the system. This image analysis technique also helps to extract detailed information regarding the nucleation, growth, and coalescence of bubbles, as well as the efficiency of CSI. Figure 5 depicts the ultimate heavy oil recovery of each test at a glance, which their values have been obtained using the image analysis technique explained before. In addition, the following sections provide an exhaustive examination of the impact of critical variables such as pressure depletion rate, solvent type, and reservoir parameters on foamy oil flow dynamics, as well as the overall effectiveness of CSI. The goal of this comprehensive study is to explore the intricate interaction between these parameters in order to clarify the role they play in shaping the behaviour of foamy oil and ultimately influencing the overall performance of the CSI process.

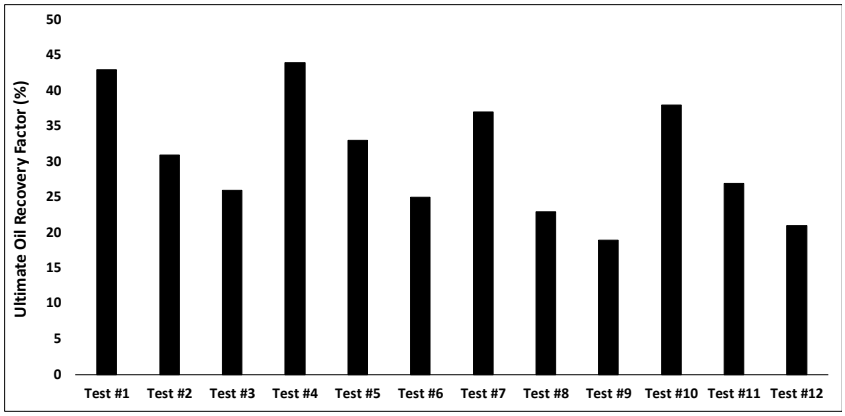

Figure 5. Ultimate heavy oil recovery of different CSI tests.

3.2.1. Effect of Solvent Type on CSI

Three distinct scenarios were analysed meticulously to evaluate the effect of solvent types on the efficiency of the CSI process in enhancing heavy oil recovery. There was a variation in composition of solvents in each scenario, with a particular emphasis on CO_2 in the solvent mixtures. The investigation revealed compelling evidence suggesting that solvents with higher CO_2 concentrations consistently yielded superior performance than their counterparts. The significance of this observation can be attributed to the multiple interplay of factors, each contributing significantly to the overall efficiency of CSI.

Firstly, the PVT analysis illustrated that CO_2 is capable of simultaneously reducing viscosity and increasing swelling factors in heavy oils. These dual mechanisms serve as potent driving forces, facilitating enhanced oil recovery. By reducing viscosity, CO_2 effectively lowers the resistance encountered during oil displacement, thereby promoting more efficient flow dynamics within the reservoir formation. Furthermore, the increased swelling factor contributes to greater reservoir saturation, which in turn results in enhanced sweep efficiency and, subsequently, higher recovery rates.

The injection of CO_2 into heavy oil reservoirs is intended to achieve a number of results, including swelling of oil, reduction in viscosity, and subsequently, the increased mobility of heavy oil. Swelling factors can have a substantial impact on the overall efficiency of a recovery process, even if they are relatively small. A volumetric expansion coupled with viscosity reduction can improve the flow characteristics and increase displacement efficiency, thereby facilitating a more efficient extraction. Even if the individual parameters show relatively small numerical changes, the combination of these factors leads to improved sweep efficiency and overall recovery factor. Furthermore, CO_2 is highly soluble, which further enhances its capability as a solvent. As a result of this increased solubility, there is a higher concentration of gas molecules within the solvent, which promotes more effective interactions between the oil phase and the gas phase. Therefore, solvents enriched with CO_2 exhibit enhanced dissolution capabilities, facilitating the mobilization and extraction of more heavy oil from reservoirs.

Experimental results from the microfluidic tests confirm the observations made above. In Test #1, a pure CO_2 solvent was utilised under specific conditions including a pressure depletion rate of 12 kPa/min and a porosity of 47%, which demonstrated a notable recovery of 43%. Regarding the oil recovery measurement, using the robust image analysis technique described earlier, oil recovery was quantified by delineating and counting pixels corresponding to distinct oil phases within the microfluidic system. The original image as well as the processed image related to the end of the CSI process in Test #1 is shown in Figure 6. Subsequent tests provided further insights into the effects of solvent composition on recovery. A solvent mixture comprising 75% CO_2 and 25% CH_4 resulted in a lower recovery factor of 31% in Test #2. The original image as well as the processed image related to the end of the CSI process in Test #2 is shown in Figure 7. Test #3, which utilised a solvent composition of 50% CO_2 and 50% CH_4, also showed a diminished recovery factor of 26%. The original image as well as the processed image related to the end of the CSI process in

Test #3 is shown in Figure 8. It is evident from these diminishing recovery rates that CO_2 plays a crucial role in enhancing heavy oil recovery through mechanisms such as foamy oil flow promotion, swelling, and viscosity reduction.

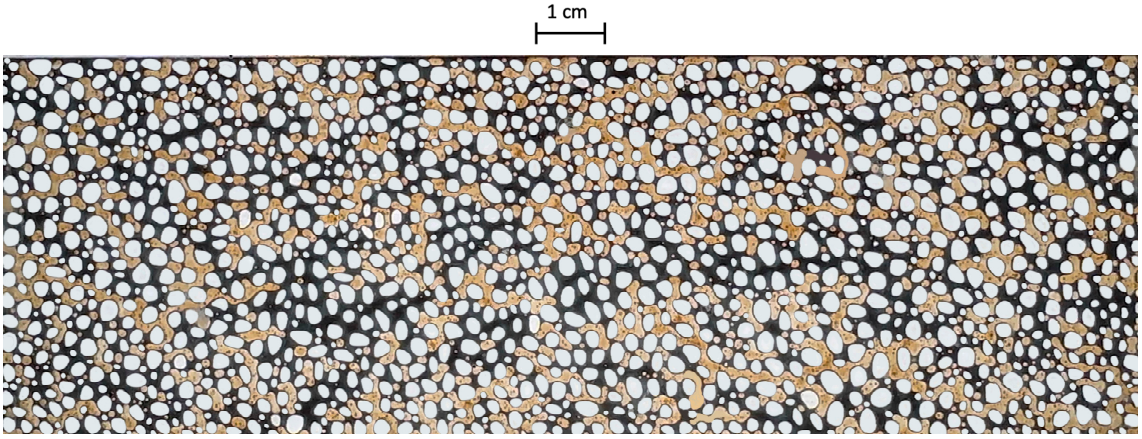

(**a**)

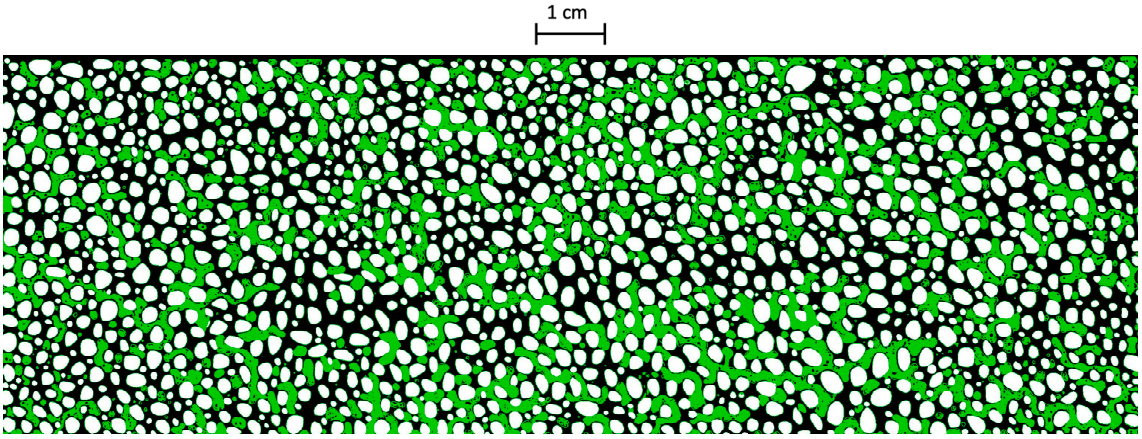

(**b**)

Figure 6. Results of the microfluidic CSI at the end of the process for Test #1 (the graphs are presented at a 1:1 scale): (**a**) original image (colour legend: black represents heavy oil, brown depicts the dispersed gas portion, and white shows the grains) and (**b**) processed image (colour legend: black represents heavy oil, green depicts the dispersed gas portion, and white shows the grains).

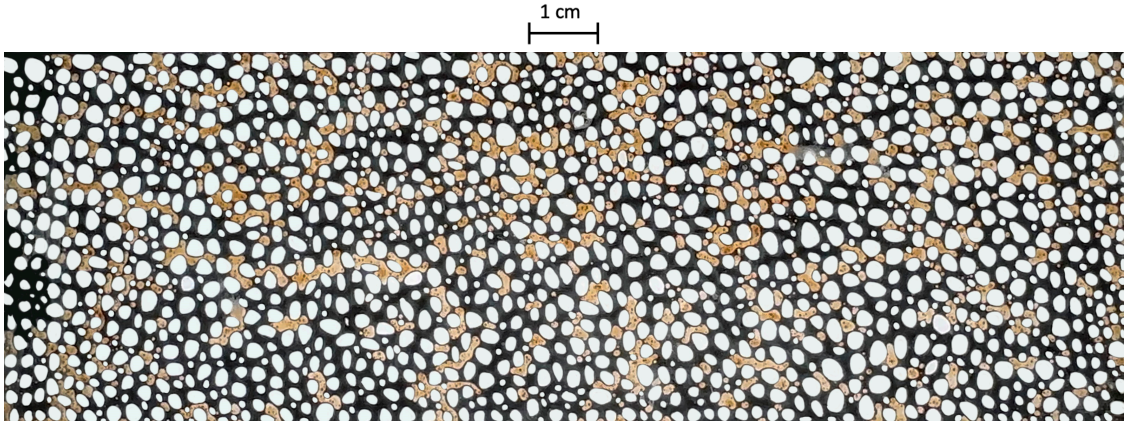

(**a**)

Figure 7. *Cont.*

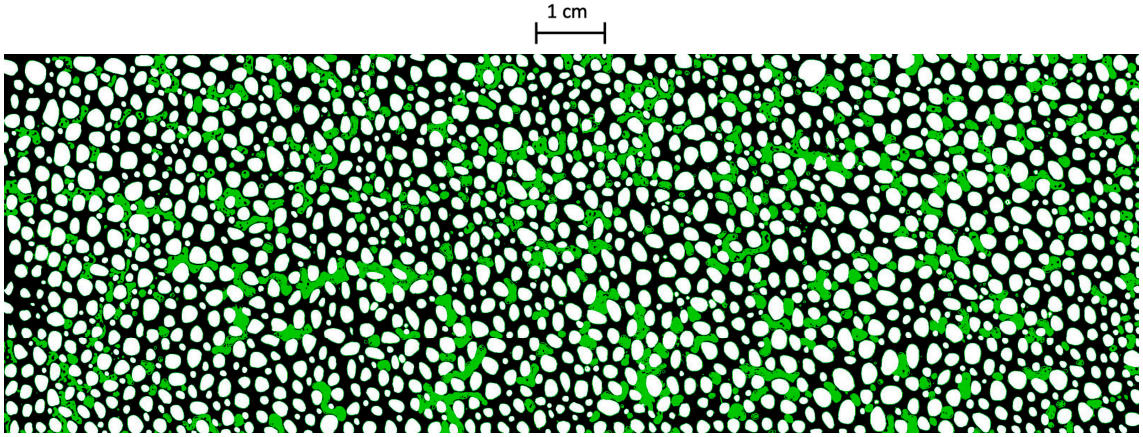

(**b**)

Figure 7. Results of the microfluidic CSI at the end of the process for Test #2 (the graphs are presented at a 1:1 scale): (**a**) original image (colour legend: black represents heavy oil, brown depicts the dispersed gas portion, and white shows the grains) and (**b**) processed image (colour legend: black represents heavy oil, green depicts the dispersed gas portion, and white shows the grains).

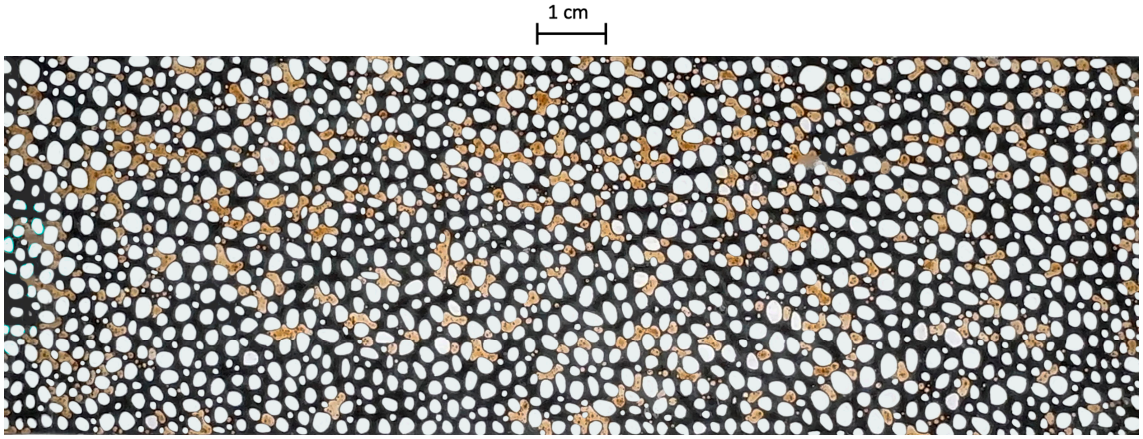

(**a**)

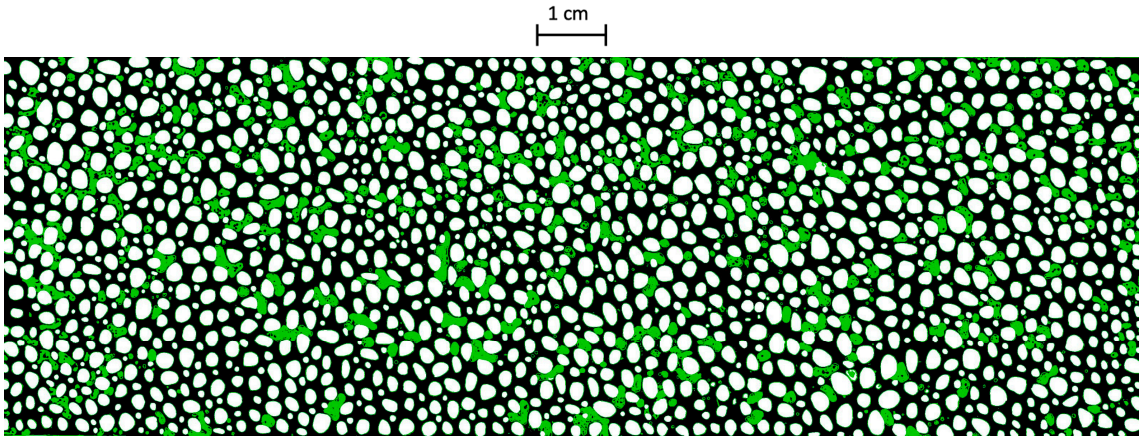

(**b**)

Figure 8. Results of the microfluidic CSI at the end of the process for Test #3 (the graphs are presented at a 1:1 scale): (**a**) original image (colour legend: black represents heavy oil, brown depicts the dispersed gas portion, and white shows the grains) and (**b**) processed image (colour legend: black represents heavy oil, green depicts the dispersed gas portion, and white shows the grains).

These comprehensive analysis highlights the critical role that solvent composition, particularly the concentration of CO_2, plays in improving the efficiency of the CSI process. It is possible to maximise heavy oil recovery from challenging reservoirs by leveraging the unique physical and chemical properties of CO_2, thereby unlocking significant potential for improving heavy oil production efficiency.

3.2.2. Effect of Pressure Depletion Rate on CSI

It was observed that pressure depletion rate plays a pivotal role in controlling the dynamics of foamy oil flow and, consequently, the overall efficiency of heavy oil recovery mechanisms. Using meticulous experimentation and analysis, it has been discovered that pressure depletion rates affect foamy oil behaviour profoundly within the porous media. Higher pressure depletion rates are associated with a prolonged and extensive foamy oil flow.

An understanding of the underlying mechanisms can assist in explaining this phenomenon. It has been observed that the higher the pressure depletion rate, the greater the driving force for the nucleation of bubbles within the oil phase is. It is believed that this increased driving force facilitates the formation of an increased number of gas bubbles dispersed throughout the oil, thus facilitating the creation of foamy oil conducive to enhanced oil recovery.

Furthermore, pressure depletion rates can have a significant impact on bubble coalescence dynamics in addition to their effect on bubble formation. The higher the depletion rate, the longer the duration over which individual gas bubbles remain dispersed within the oil phase, as it constrains the timeframe available for bubble coalescence. A higher depletion rate effectively delays the aggregation of dispersed gas portions into larger, interconnected bubbles by limiting the temporal window for bubble coalescence.

Comparative analyses of experimental results obtained under varying pressure depletion rates readily demonstrate these dynamics. From the microscopic perspective, images captured during microfluidic tests reveal distinct patterns that highlight the differences in foamy oil behaviour under different depletion rate conditions. When depletion rates are slower, as depicted in Figure 9, the dispersed gas portions (shown in brown colour) tend to coalesce and form interconnected networks, representing a lower quality of foamy oil flow in this test. On the other hand, in conditions of faster depletion rates, as shown in Figure 10, the dispersed gas sections (shown in brown) remain clearly distinct, indicating that bubble coalescence has been delayed, which results in a higher quality of foamy oil flow.

The images depicted in Figures 9 and 10 correspond to Test #10 and Test #4, respectively. It is imperative to underscore that these images were captured from identical locations within the porous media. Furthermore, it is noteworthy that both images were acquired under exact same pressure conditions, marking the end of the experimental process.

Further comparative analysis between Test #4 and Test #10 was conducted in order to provide further insights into the impact of pressure depletion rates on the overall performance of the CSI. As it was demonstrated in Table 2, these two tests were conducted under similar conditions, except for varying pressure depletion rates.

Test #4, which involved accelerated pressure depletion, achieved a remarkable recovery factor of 44%, demonstrating the effectiveness of accelerated pressure depletion in the recovery of heavy oil. Figure 11 shows the original as well as the processed images related to the end of Test #4.

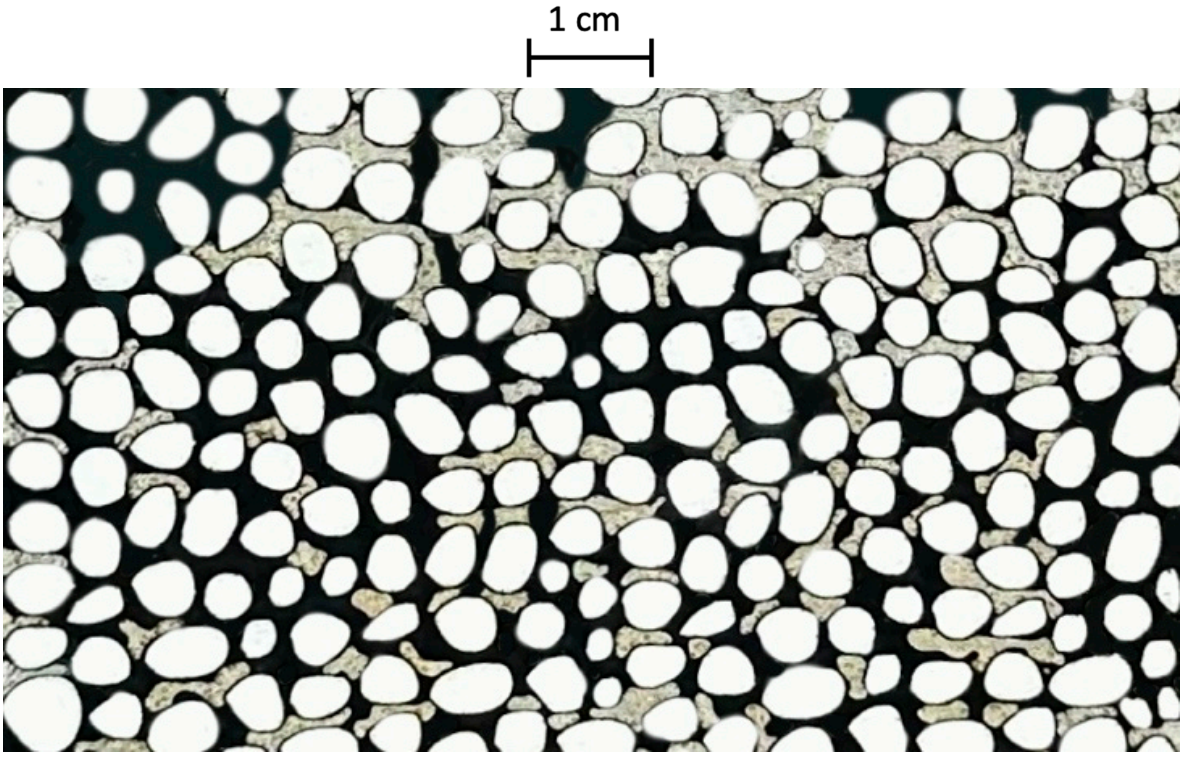

Figure 9. Effect of slow pressure depletion rate on foamy oil flow behaviour in Test #10 (the graph is presented at a 2:1 scale). (Colour legend: black represents heavy oil, brown depicts the dispersed gas portion, and white shows the grains).

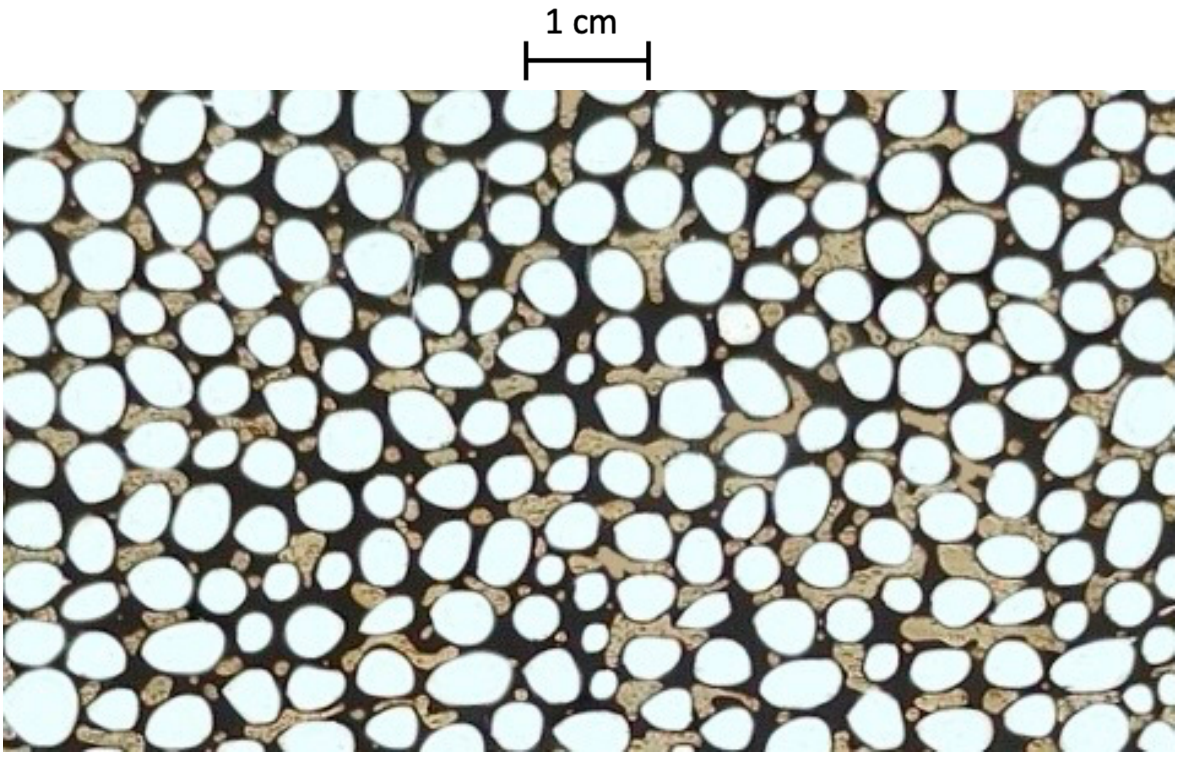

Figure 10. Effect of slow pressure depletion rate on foamy oil flow behaviour in Test #4 (the graph is presented at a 2:1 scale). (Colour legend: black represents heavy oil, brown depicts the dispersed gas portion, and white shows the grains).

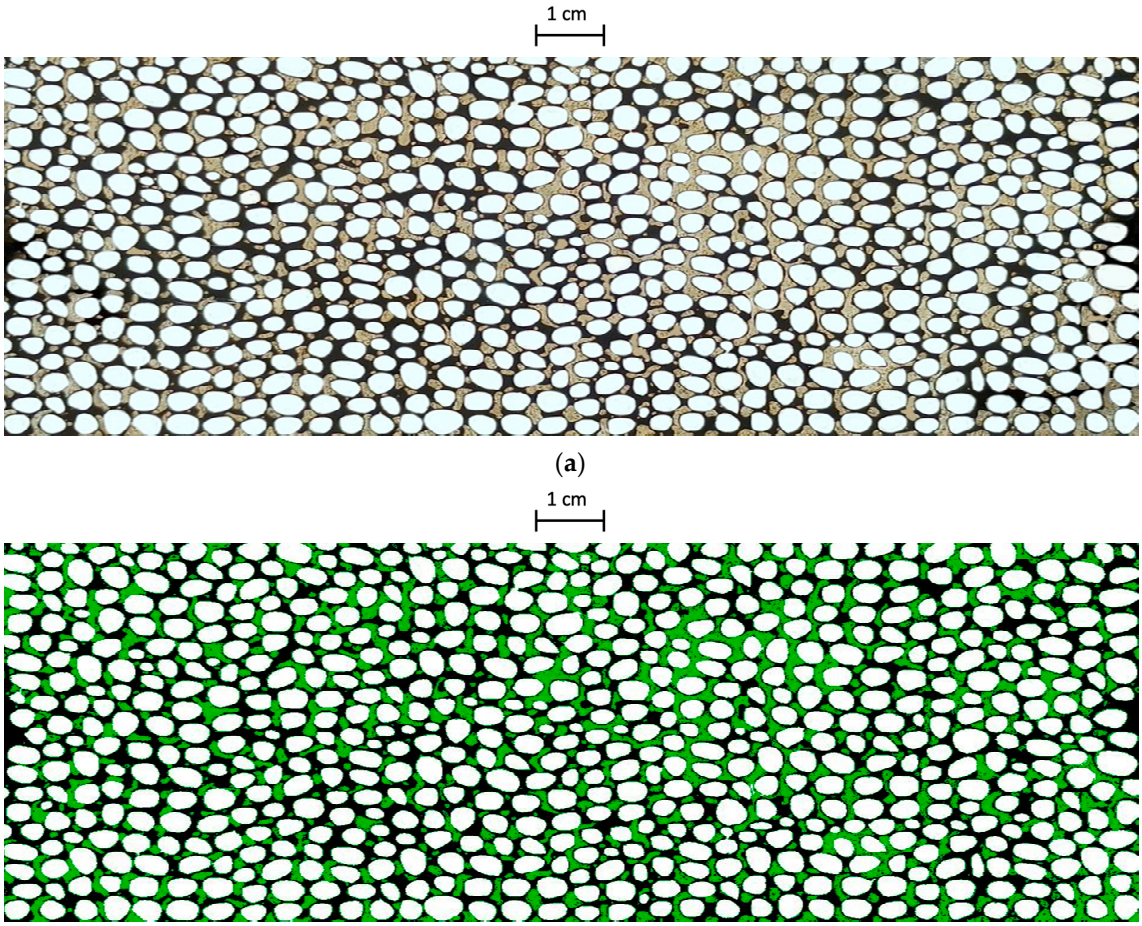

Figure 11. Results of the microfluidic CSI at the end of the process for Test #4 (the graphs are presented at a 1:1 scale): (**a**) original image (colour legend: black represents heavy oil, brown depicts the dispersed gas portion, and white shows the grains) and (**b**) processed image (colour legend: black represents heavy oil, green depicts the dispersed gas portion, and white shows the grains).

Alternatively, in Test #10, which had a lower pressure depletion rate, the recovery factor decreased to 38%, indicating a significant reduction in the overall performance of the process. Figure 12 shows the original as well as the processed images related to the end of Test #10.

These discrepancies in recovery outcomes highlight the crucial role played by pressure depletion rates in shaping the dynamics of foamy oil flow and, thereby, affecting overall recovery efficiency. The insights gained from such analyses can be utilised to optimise CSI processes and unlock the full potential of the CSI process by manipulating pressure depletion rates.

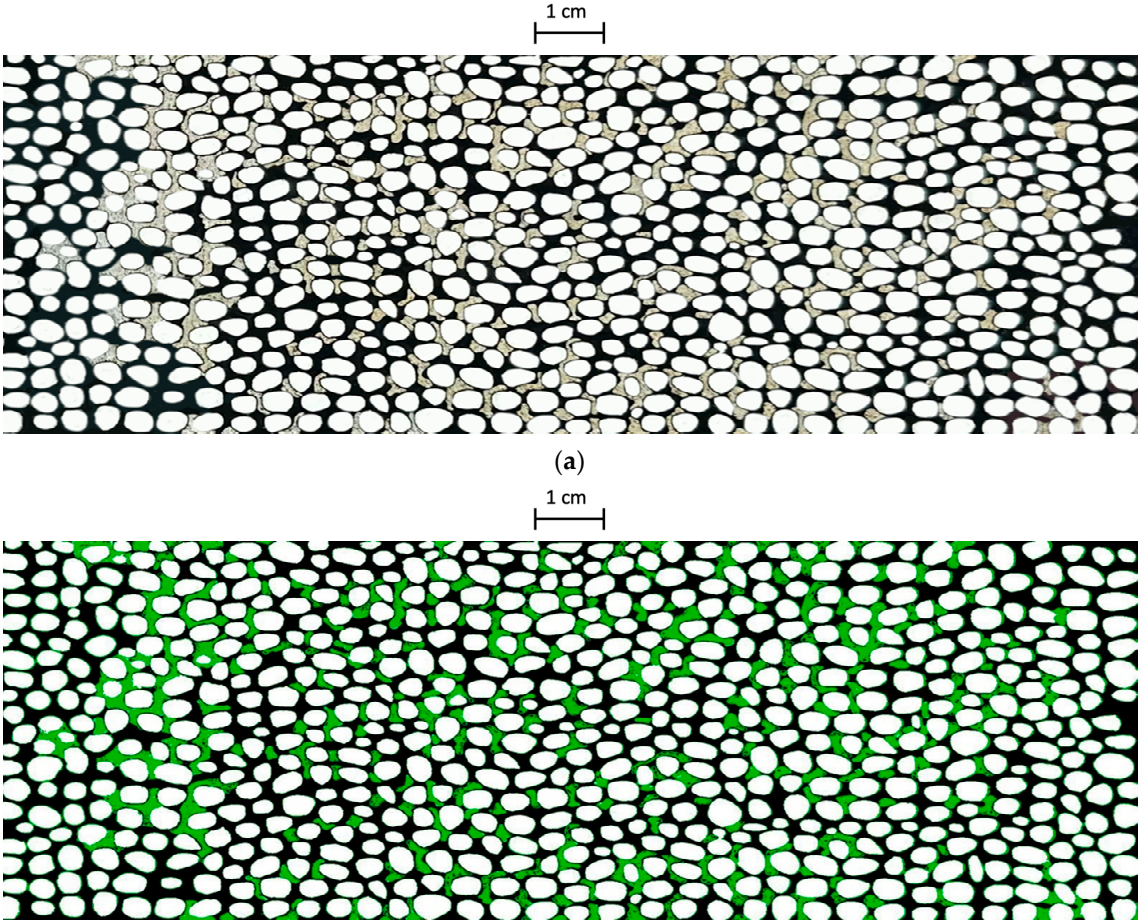

Figure 12. Results of the microfluidic CSI at the end of the process for Test #10 (the graphs are presented at a 1:1 scale): (**a**) original image (colour legend: black represents heavy oil, brown depicts the dispersed gas portion, and white shows the grains) and (**b**) processed image (colour legend: black represents heavy oil, green depicts the dispersed gas portion, and white shows the grains).

3.2.3. Effect of Reservoir Parameters on CSI

The observations also demonstrate the importance of porosity in extending foamy oil flow dynamics. Lower porosity within the reservoir acts as a barrier against the movement of bubbles, effectively delaying their coalescence and improving the quality of foamy oil flow. The phenomenon was visualised in a comparative analysis of two different microfluidic CSI tests, in which conditions remained consistent with the exception of variations in porosity levels of 32% and 47%.

In Figure 13, corresponding to 32% porosity, foamy oil quality appeared superior, with distinct separation among bubbles.

Conversely, Figure 14, representing 47% porosity, showcased connected bubbles, indicating a lower quality of foamy oil. This visual contrast underscores the significant impact of porosity on the foamy oil flow dynamics and CSI performance.

Moreover, to elucidate the influence of reservoir parameters comprehensively, a comparative analysis of Test #1 and Test #4 was conducted. These tests, identical in all aspects except for variations in reservoir parameters, yielded notable recovery rates. Test #4, characterised by 32% porosity and permeability of 5.6 Darcy, attained a recovery rate of 44%, whereas Test #1, with porosity of 47% and permeability of 8.7 Darcy, achieved a slightly lower recovery rate of 43%.

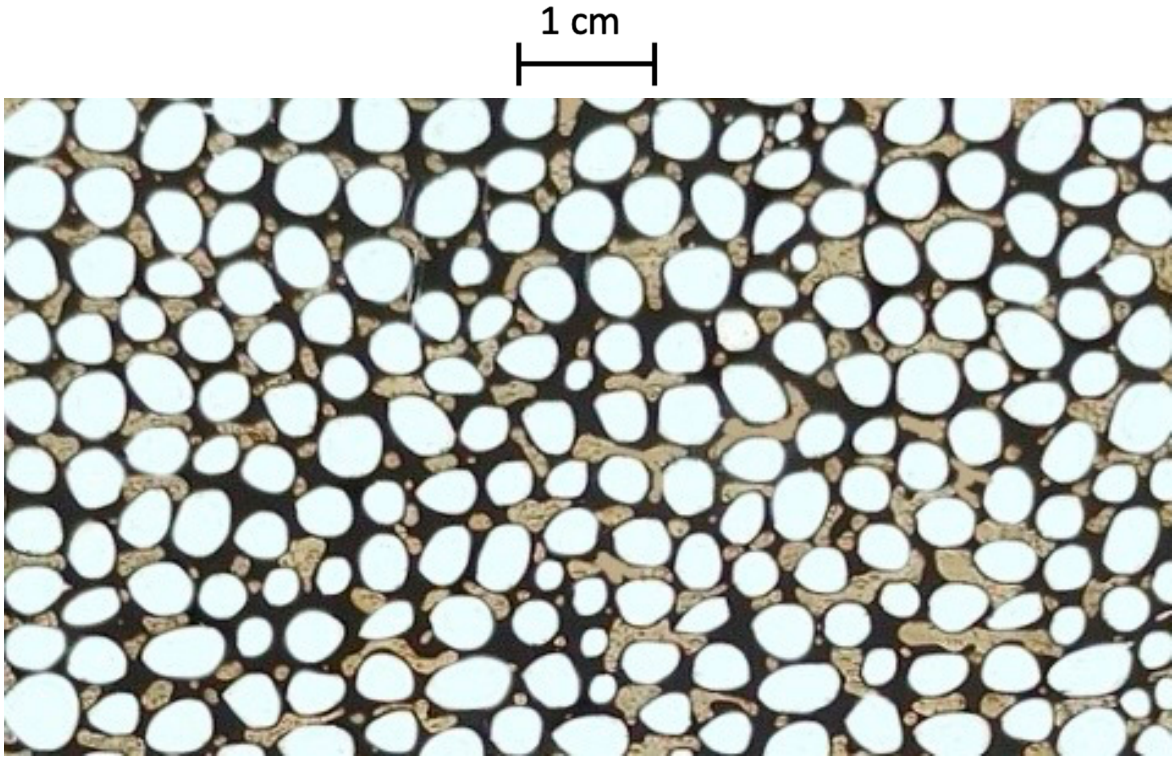

Figure 13. Effect of reservoir parameters (lower porosity and lower permeability) on foamy oil flow behaviour in Test #4 (the graph is presented at a 1:2 scale). (Colour legend: black represents heavy oil, brown depicts the dispersed gas portion, and white shows the grains).

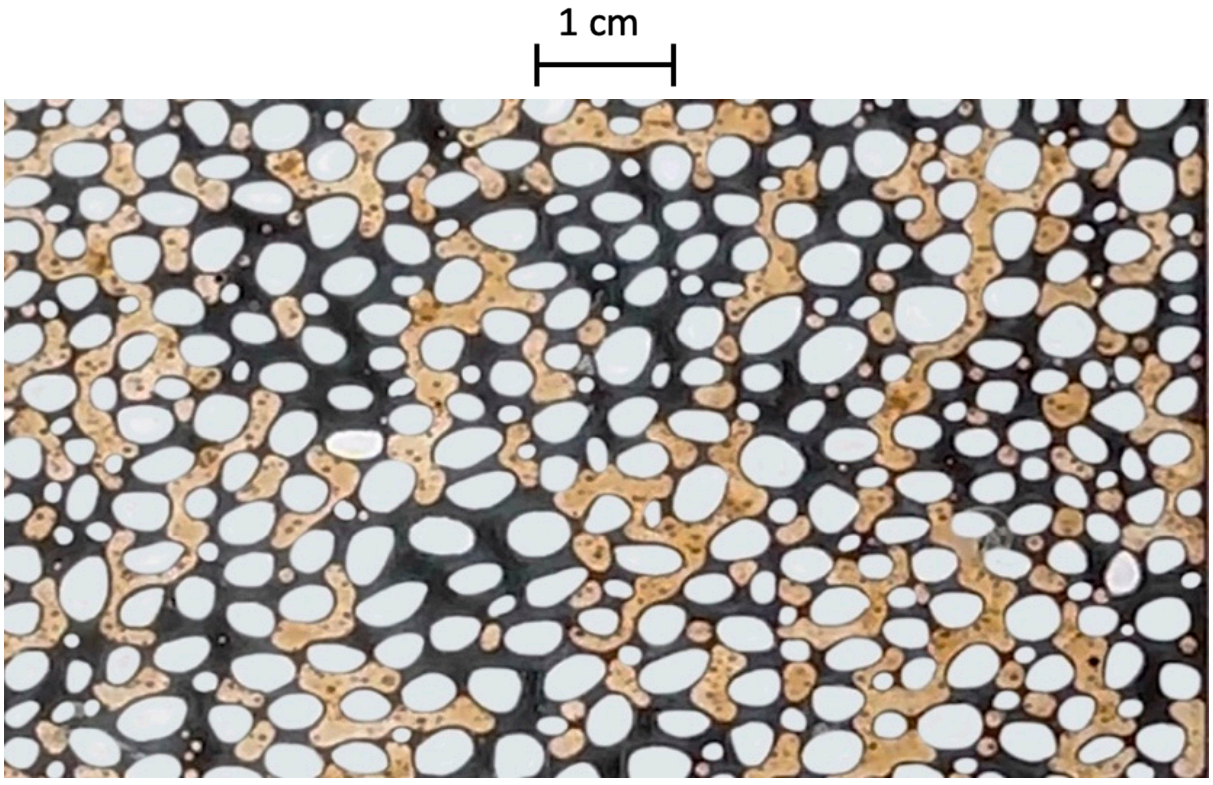

Figure 14. Effect of reservoir parameters (higher porosity and higher permeability) on foamy oil flow behaviour in Test #1 (the graph is presented at a 1:2 scale). (Colour legend: black represents heavy oil, brown depicts the dispersed gas portion, and white shows the grains).

In addition to porosity, the permeability of the reservoir also plays an important role in shaping the performance of the process. The higher the permeability of the reservoir, the greater the overall foamy oil mobility within the reservoir, thereby affecting the recovery rate and efficiency. The intricate interplay between porosity and permeability underscores the multifaceted nature of reservoir dynamics and their profound implications for oil recovery processes.

3.3. Simulation Results

The CSI process has also been thoroughly investigated from a numerical perspective in this project. First, a PVT model using CMG WINPROP (2021.10) has been tuned using the experimental PVT results presented earlier. Figures 15–23 demonstrate the comparison between the experimental PVT results and CMG WINPROP (2021.10) model.

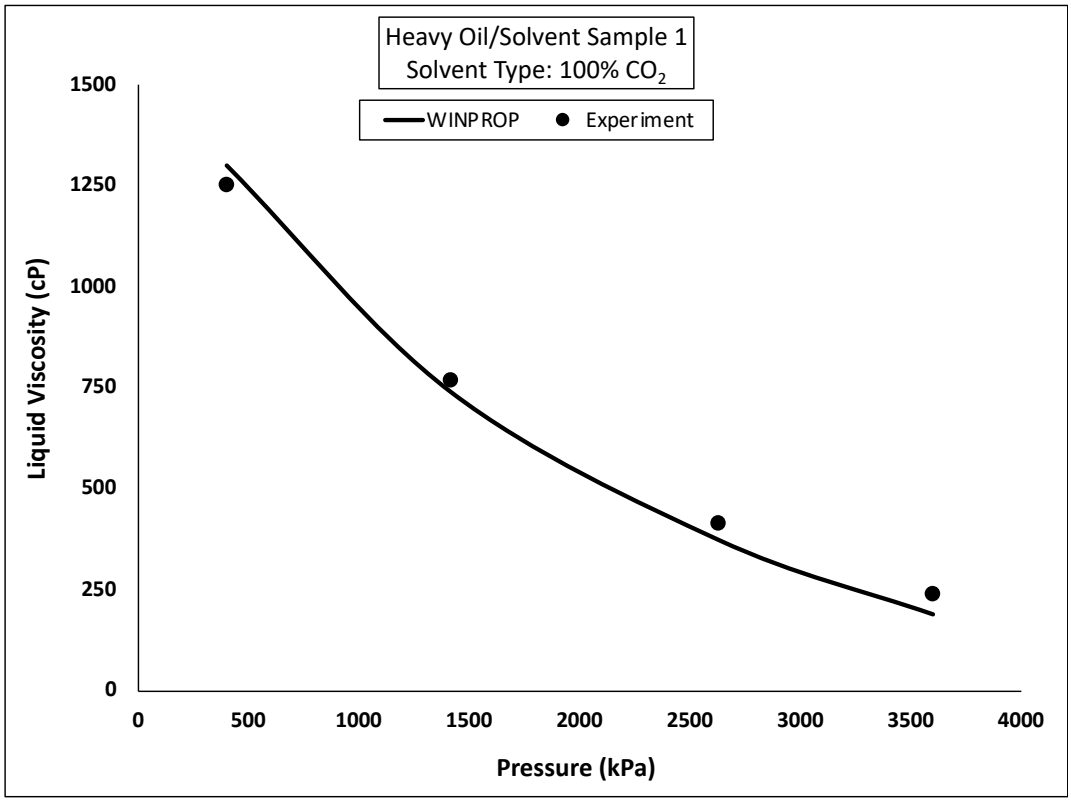

Figure 15. Comparison between experimental and WINPROP results for liquid viscosity as a function of pressure for heavy oil/solvent sample 1.

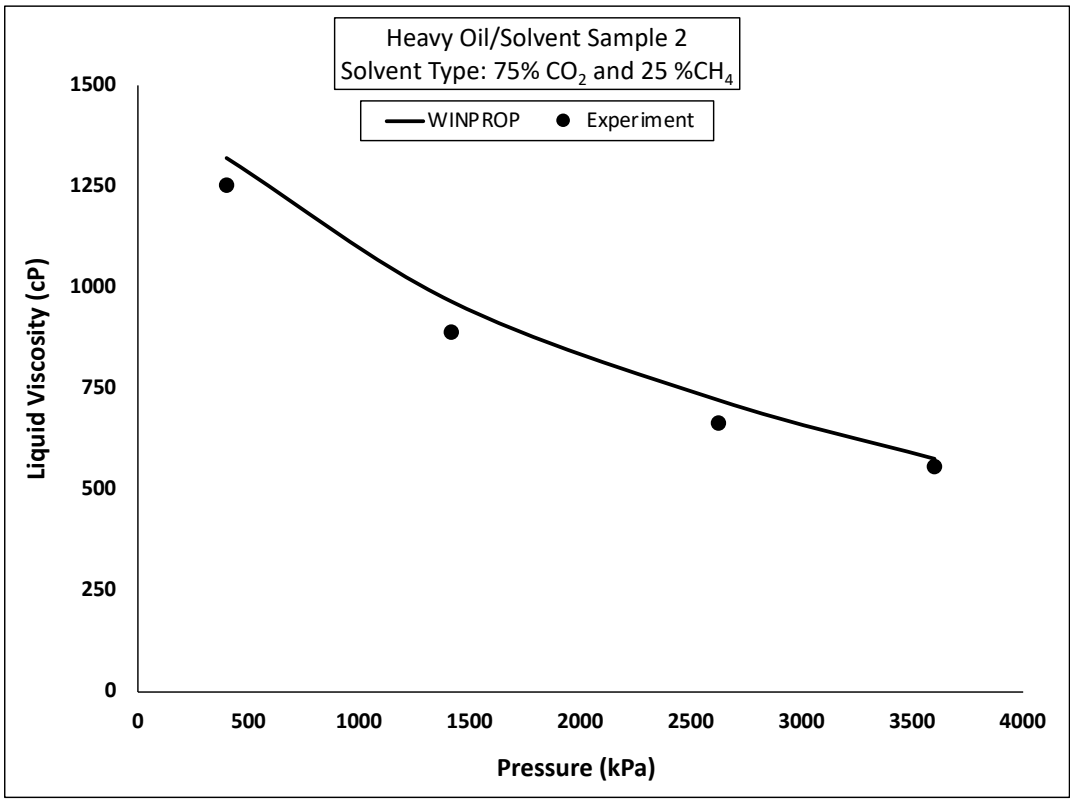

Figure 16. Comparison between experimental and WINPROP results for liquid viscosity as a function of pressure for heavy oil/solvent sample 2.

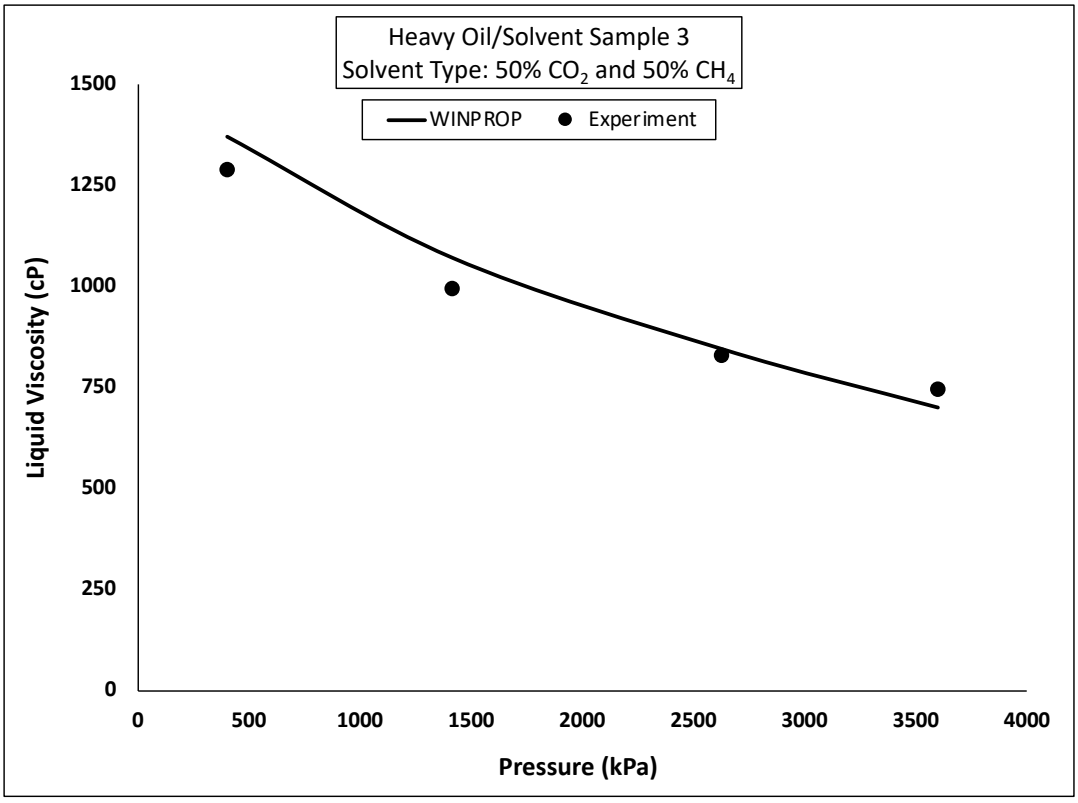

Figure 17. Comparison between experimental and WINPROP results for liquid viscosity as a function of pressure for heavy oil/solvent sample 3.

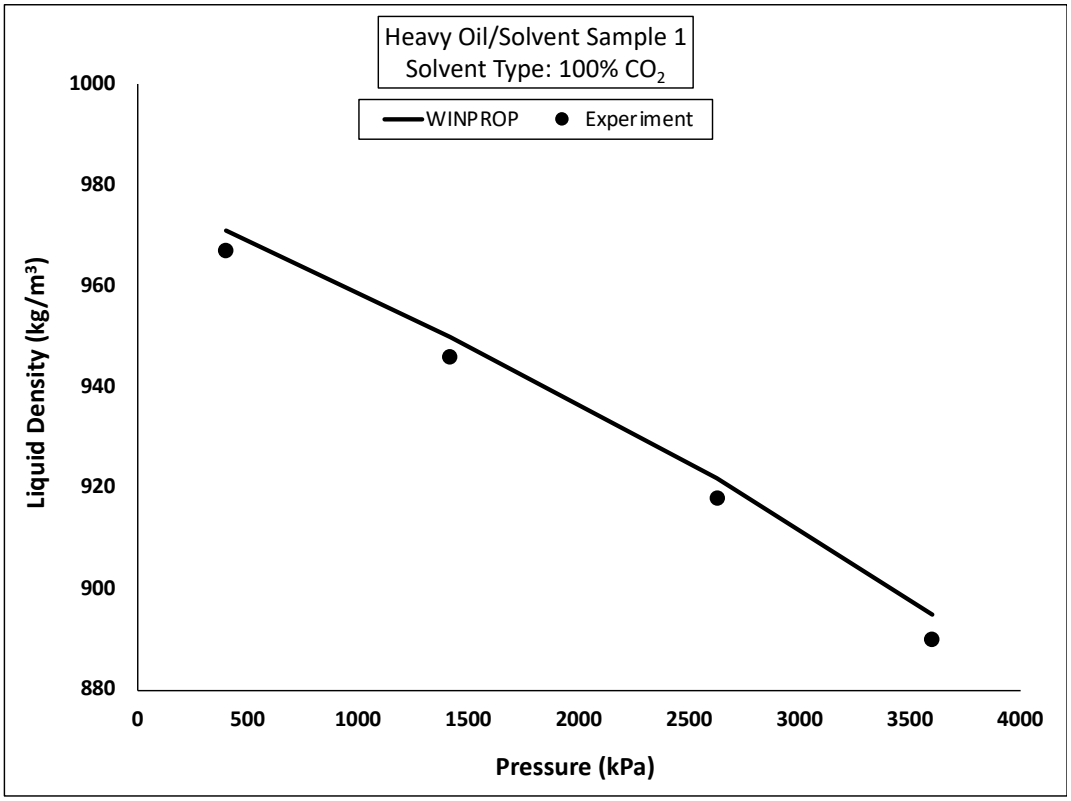

Figure 18. Comparison between experimental and WINPROP results for liquid density as a function of pressure for heavy oil/solvent sample 1.

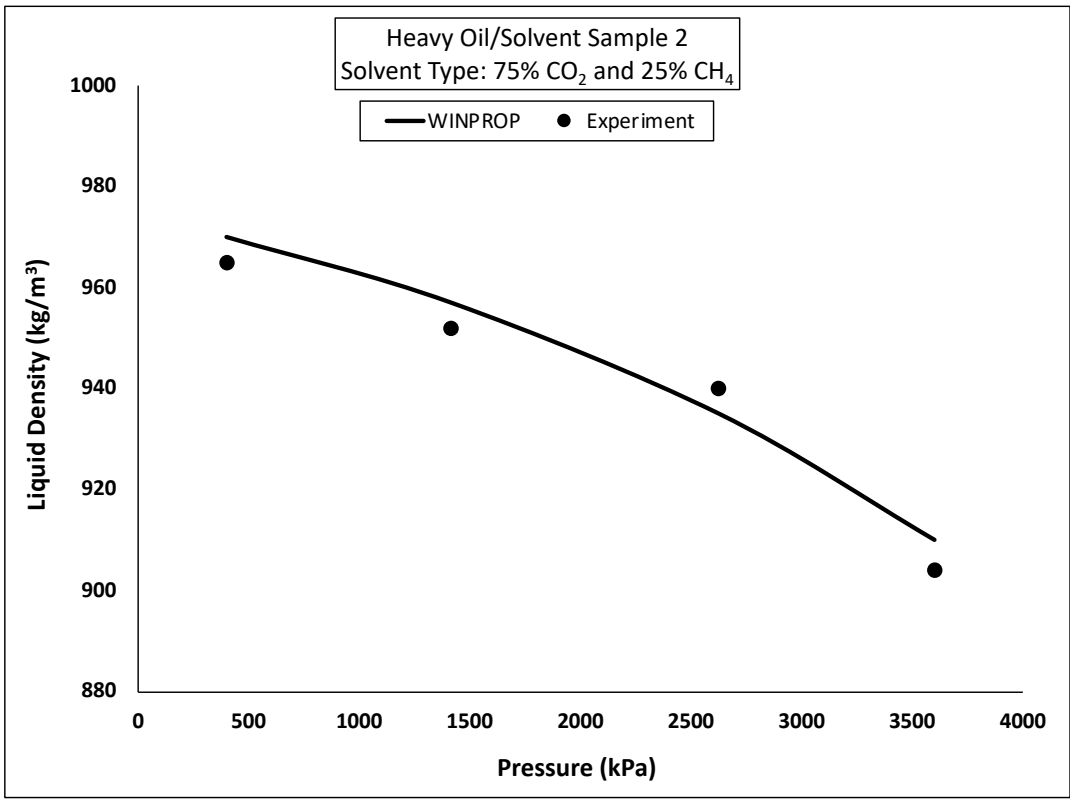

Figure 19. Comparison between experimental and WINPROP results for liquid density as a function of pressure for heavy oil/solvent sample 2.

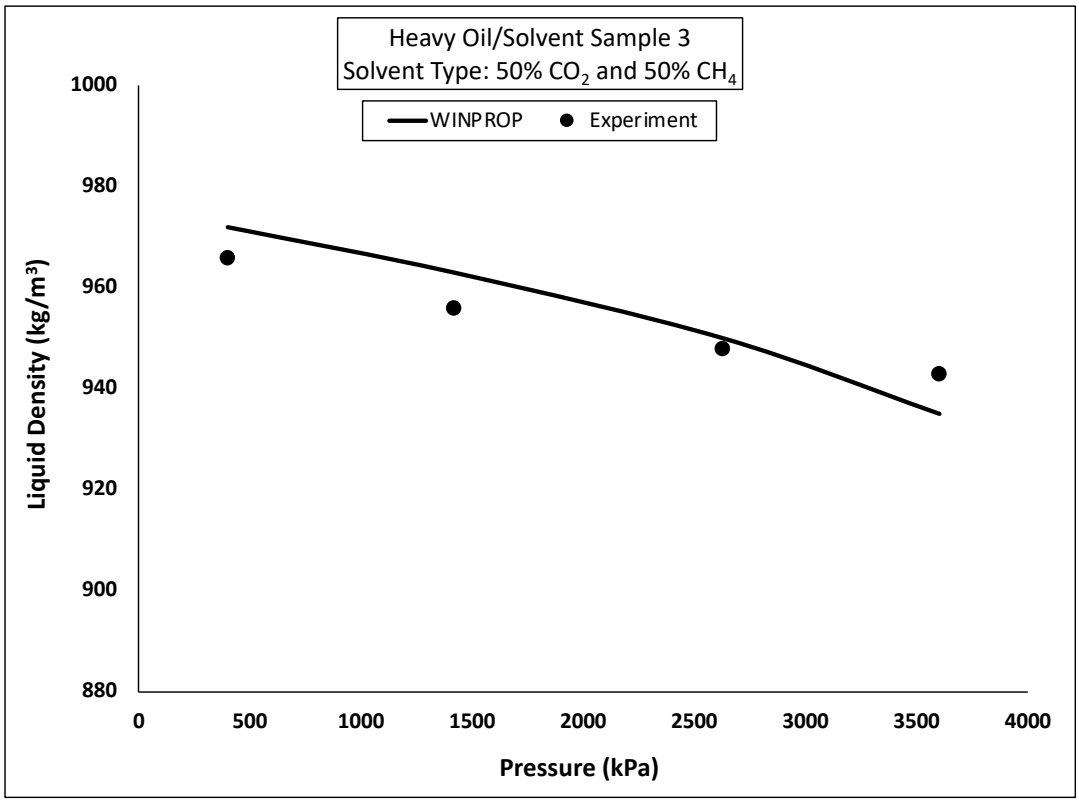

Figure 20. Comparison between experimental and WINPROP results for liquid density as a function of pressure for heavy oil/solvent sample 3.

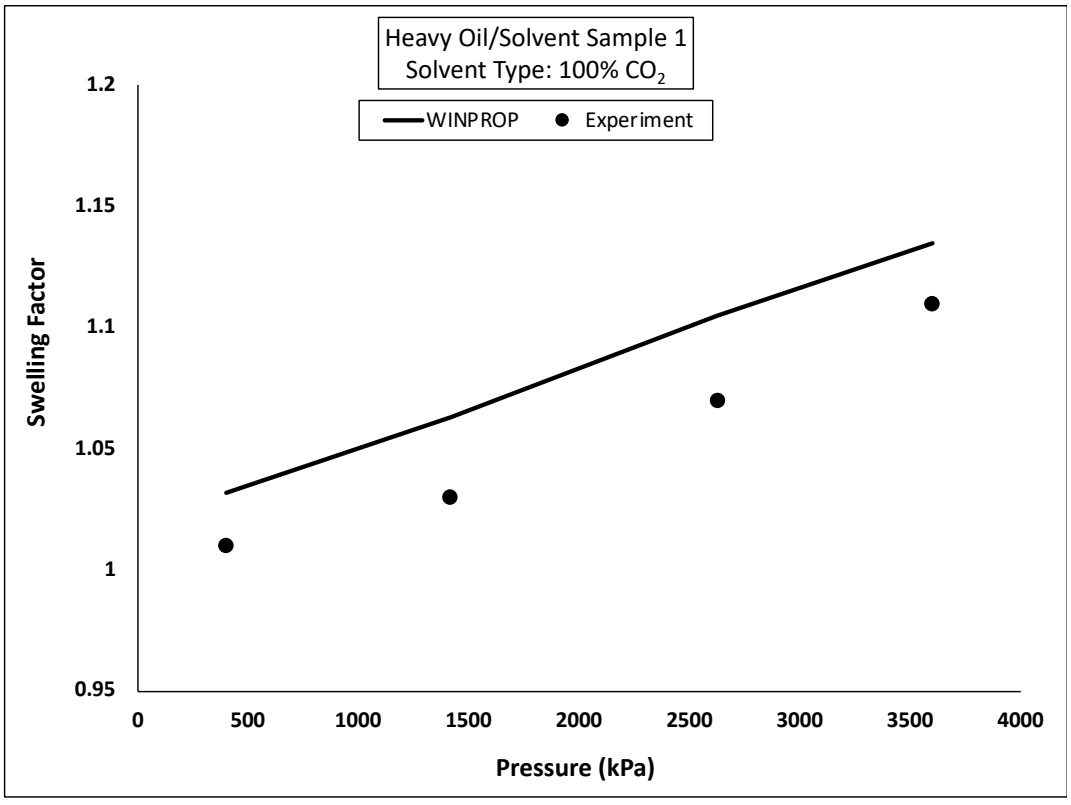

Figure 21. Comparison between experimental and WINPROP results for swelling factor as a function of pressure for heavy oil/solvent sample 1.

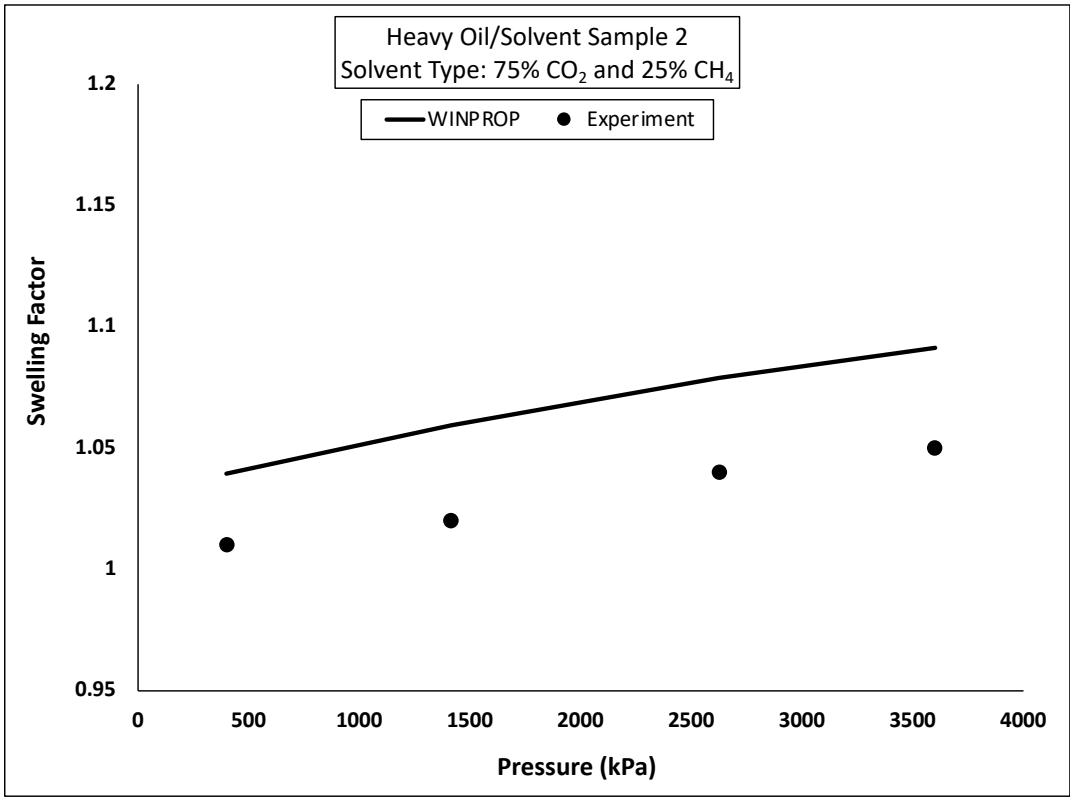

Figure 22. Comparison between experimental and WINPROP results for swelling factor as a function of pressure for heavy oil/solvent sample 2.

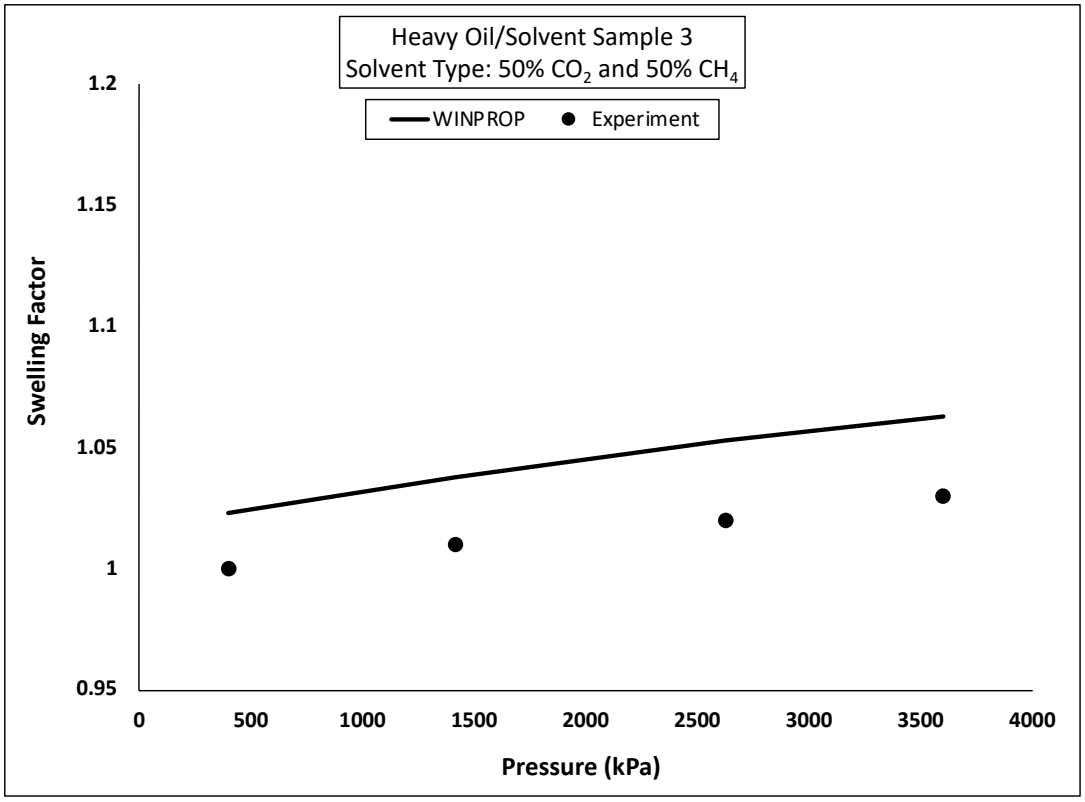

Figure 23. Comparison between experimental and WINPROP results for swelling factor as a function of pressure for heavy oil/solvent sample 3.

Figures 15–23 illustrate vividly how the experimental measurements and WINPROP's predictive abilities are in excellent alignment. This convergence indicates that the constructed PVT model has a strong foundation, which confirms its reliability and accuracy when simulating heavy oil recovery processes. Through the use of the reliable PVT model, the simulated CSI process can be closely matched to the experimental findings, thereby improving the accuracy and applicability of the simulation results. Using this reliable PVT model, crucial properties of the CSI process have been thoroughly extracted and integrated into the CMG STARS (2021.10) model.

As mentioned earlier, CMG STARS (2021.10) was utilised to construct a simulation model capable of replicating the CSI tests. The main reservoir parameters used in this model are presented in Table 6.

Table 6. Reservoir properties.

Parameter	Value
Model length	15 cm
Model width	5 cm
Model thickness	0.1 cm
Permeability	8.7 Darcy for Microfluidic system 1
	5.6 Darcy for Microfluidic system 2
Porosity	47% Microfluidic system 1
	32% for Microfluidic system 2
Initial pressure	1500 kPa
Initial oil saturation	100%
Initial free gas saturation	0
Initial water saturation	0
Reservoir temperature	21 °C

In order to simulate pressure depletion, a production well was defined to gradually reduce bottom-hole pressure from 1500 kPa to atmospheric pressure. As for the simulator calibration, gas–oil relative permeability, diffusion coefficients, and kinetic model parameters were adjusted, with the aid of CMG CMOST (2021.10), so that the heavy oil recoveries align with the experimental findings. The tuned diffusion coefficients for CO_2, 75% CO_2/25% CH_4, and 50% CO_2/50% CH_4 solvents were $7.1 \times 10^{-9} \frac{m^2}{s}$ and $5.1 \times 10^{-9} \frac{m^2}{s}$, and $3.1 \times 10^{-9} \frac{m^2}{s}$, respectively. In addition, Figure 24 shows the tuned relative permeability curves.

The numerical model constructed was found to be accurate in tuning heavy oil recoveries with an average relative error of 7.7%. Figure 25 presents an overview of the comparison between the ultimate oil recoveries for all 12 CSI scenarios, contrasting the experimental findings with simulation outputs.

Figures 26–37 illustrate the contrast in heavy oil recovery over time, displaying both microfluidic and simulation results for Test #1 through Test #12.

It is evident that Figure 26 through Figure 37 provide a comprehensive description of the convergence between experimental findings and simulation results, demonstrating a commendable alignment with an average relative error of 7.7%. However, it is important to acknowledge that these discrepancies stem largely from the underlying assumptions. One of the primary assumptions that can influence simulation outcomes pertains to the treatment of foamy oil viscosity. Foamy oil was assumed to have the same viscosity as heavy oil/solvent under varying pressure conditions. While convenient, this assumption introduces a potential source of error that should be carefully examined. Furthermore, in the context of history matching, it was assumed that all scenarios adhered to identical relative permeability curves.

A deeper analysis of both experimental and simulation results reveals that a heightened pressure depletion rate is associated with an accelerated increase in heavy oil recovery. Figures 38 and 39 provide an excellent illustration of this phenomenon.

Figure 38 illustrates a significant rise in section 2 of the recovery curve corresponding to Test #4, indicating rapid pressure depletion. On the other hand, Figure 39 corresponding to Test #10, characterised by a slower depletion rate, exhibits a more gradual ascent in its section 2 recovery curve. Moreover, both Test #4 and Test #10 exhibit relatively modest increases in their recovery curves across sections 1 and 3. There is an evident increase in the recovery factor curve during situations of rapid depletion, which can be attributed to the influence of heightened depletion rates on the prevention of coalescence processes. As a result of these insights, we have an increased understanding of the intricate interplay between pressure dynamics and recovery mechanisms, which provides a valuable insight into the pivotal factors that influence the foamy oil flow dynamics and the performance of the CSI process.

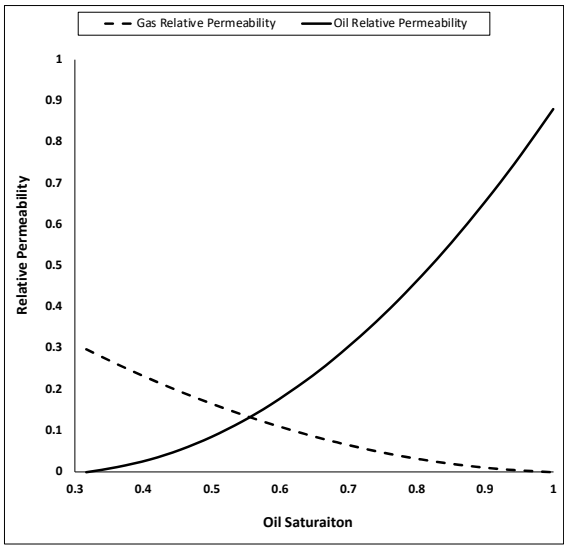

Figure 24. Tuned relative permeability curves.

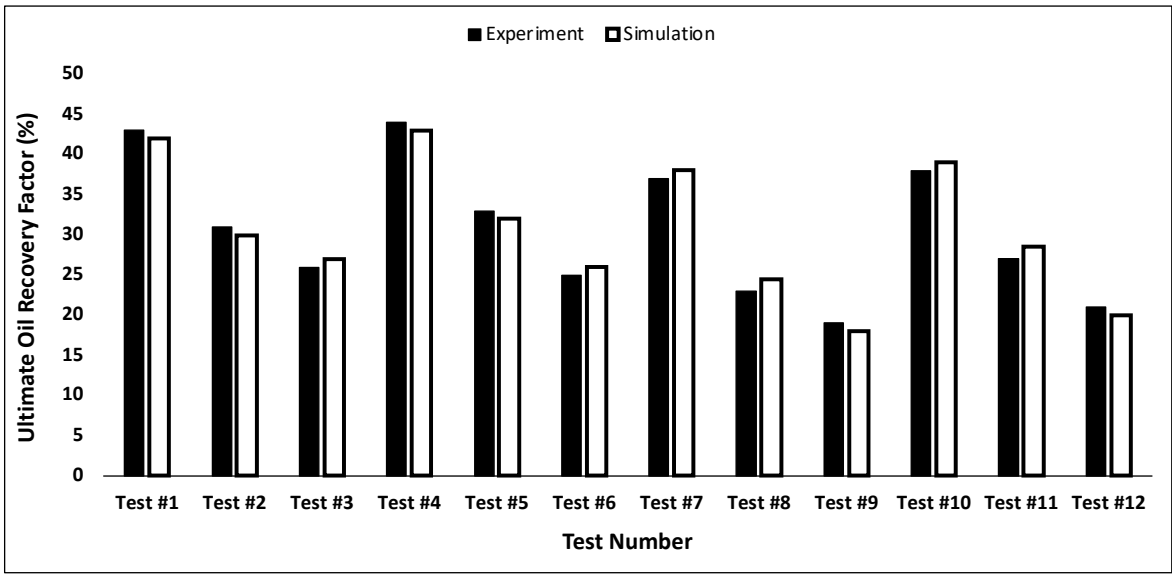

Figure 25. Comparative analysis of ultimate heavy oil recovery between experimental data and simulation outputs.

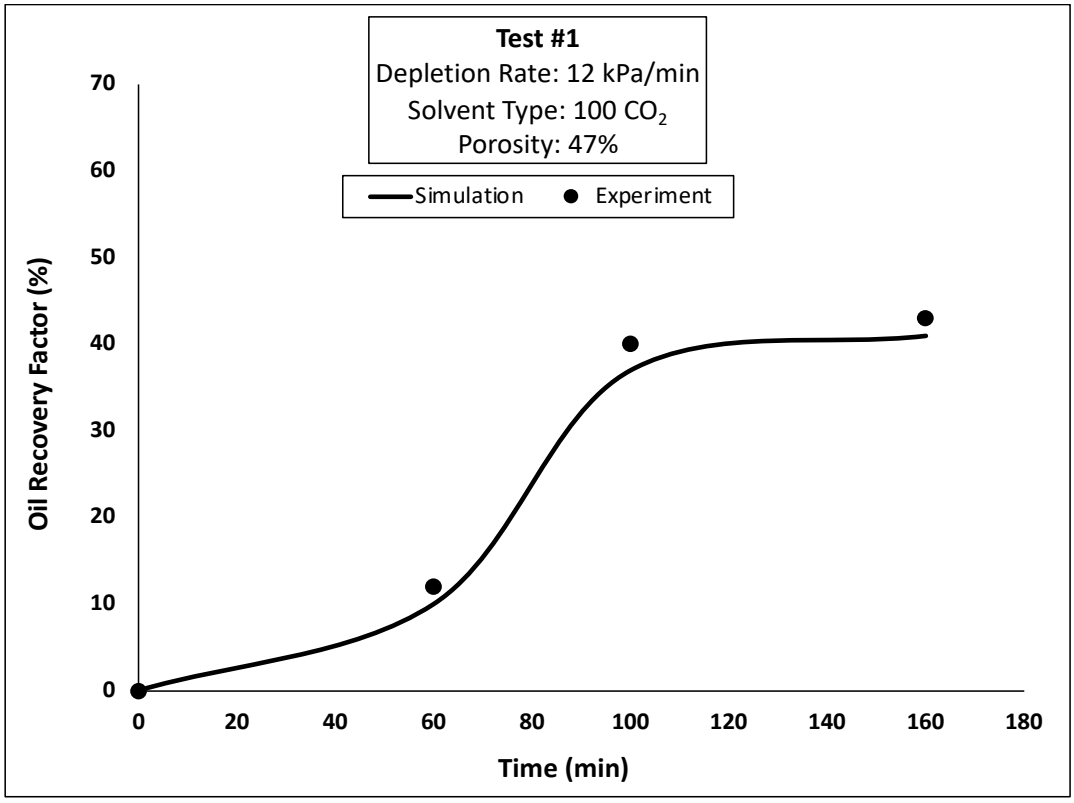

Figure 26. Comparison between the heavy oil recoveries over time for experiment and simulation over time for Test #1.

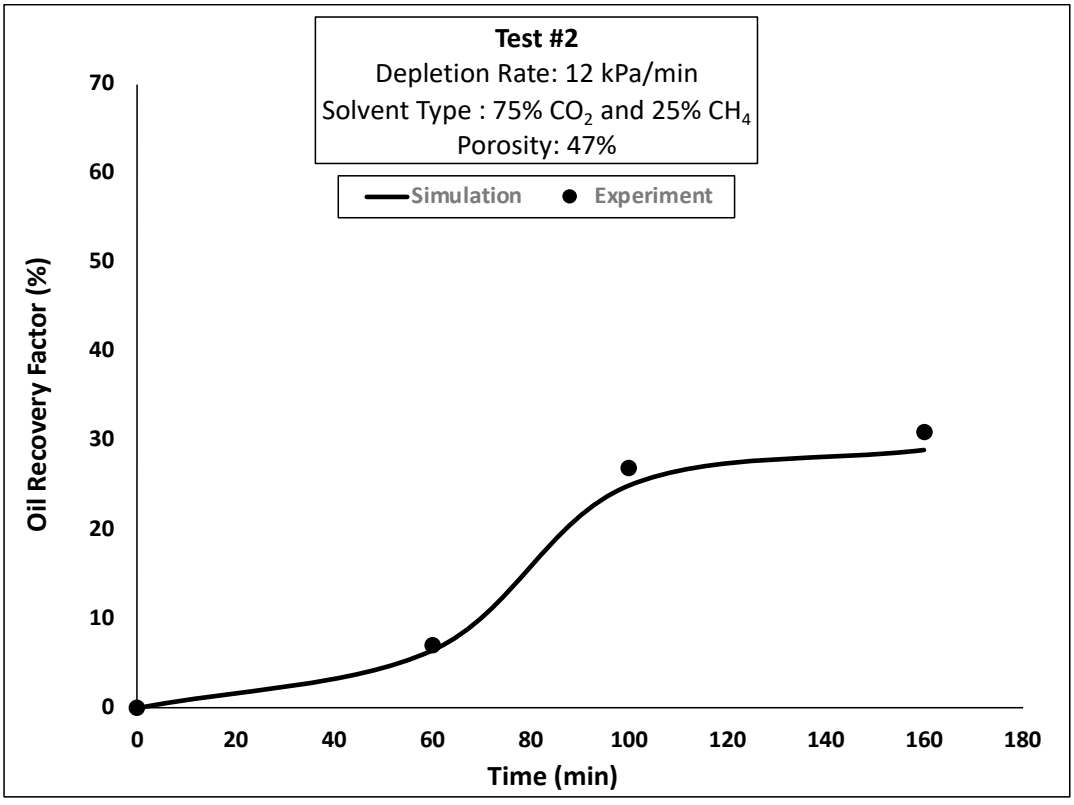

Figure 27. Comparison between the heavy oil recoveries over time for experiment and simulation over time for Test #2.

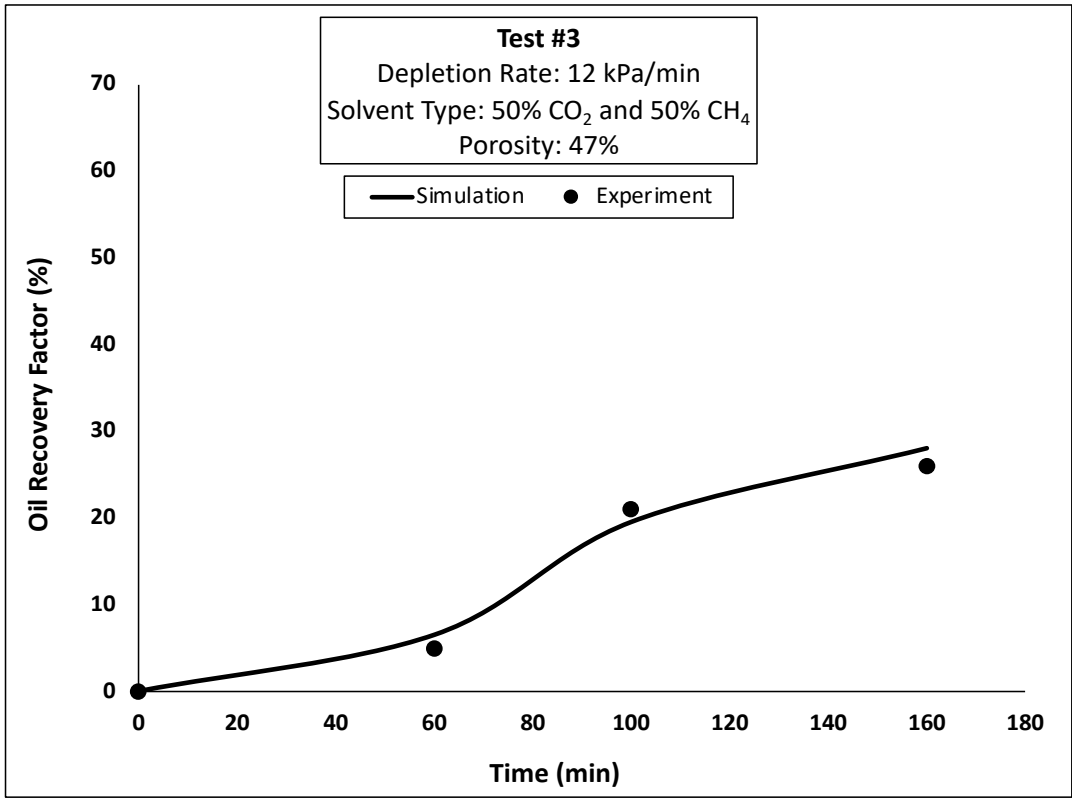

Figure 28. Comparison between the heavy oil recoveries over time for experiment and simulation over time for Test #3.

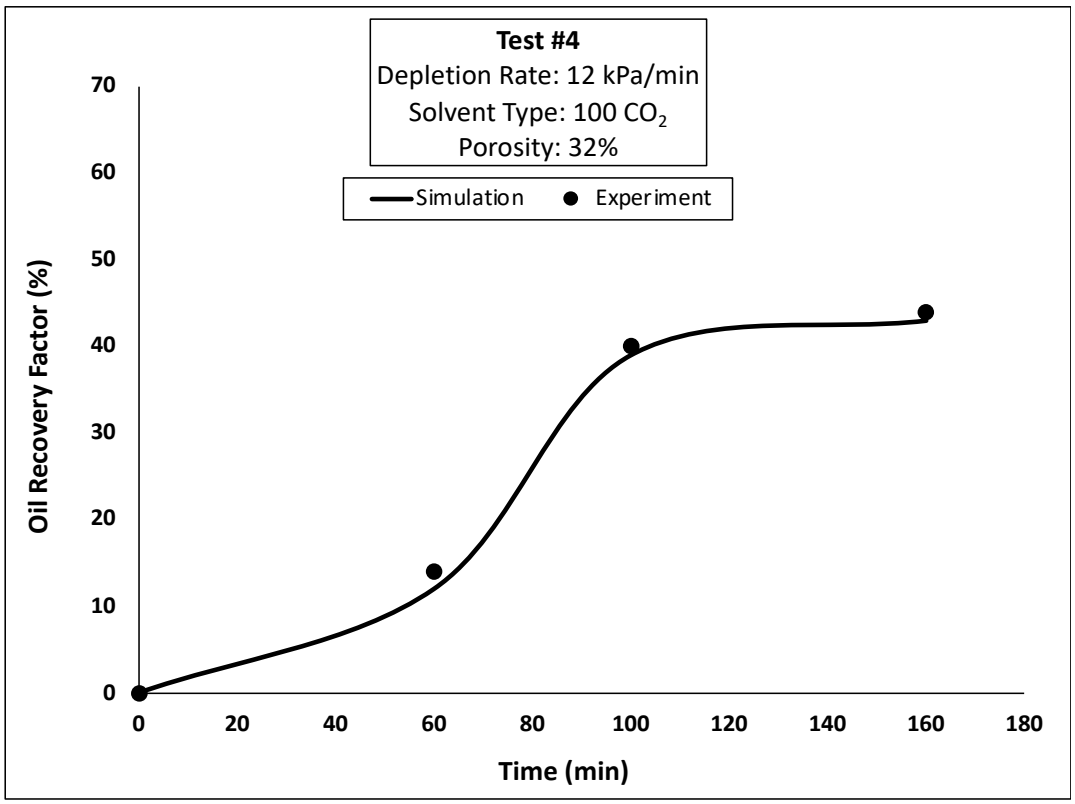

Figure 29. Comparison between the heavy oil recoveries over time for experiment and simulation over time for Test #4.

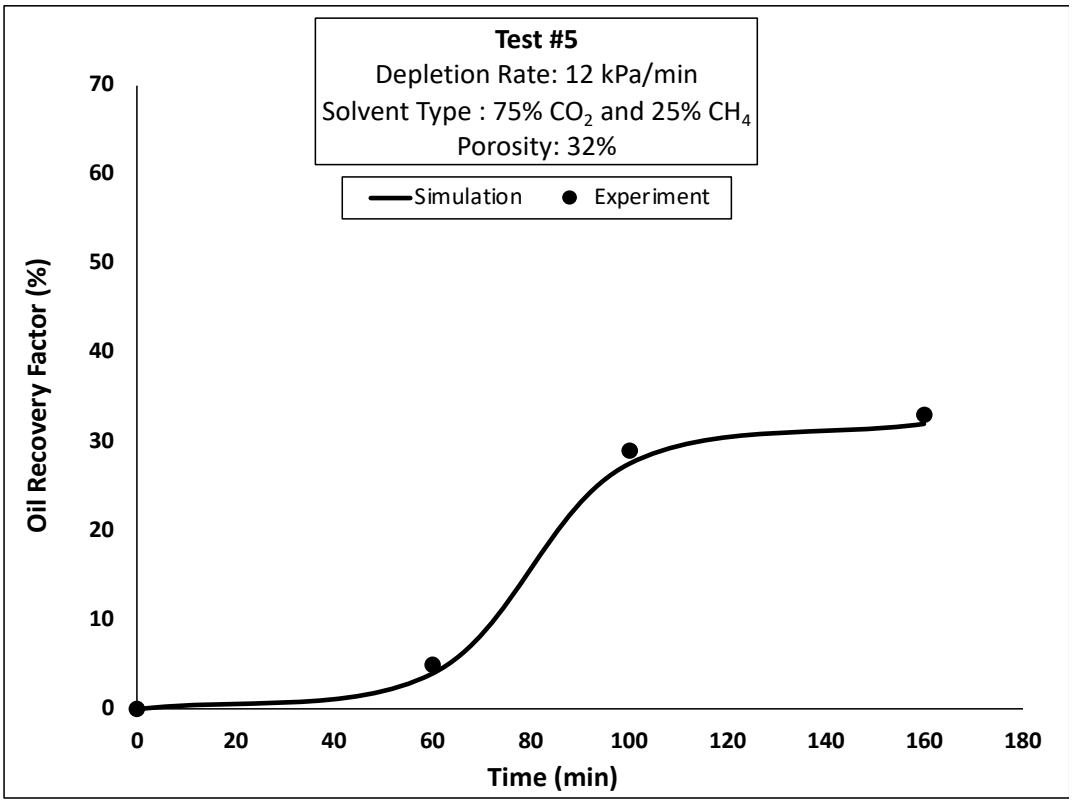

Figure 30. Comparison between the heavy oil recoveries over time for experiment and simulation over time for Test #5.

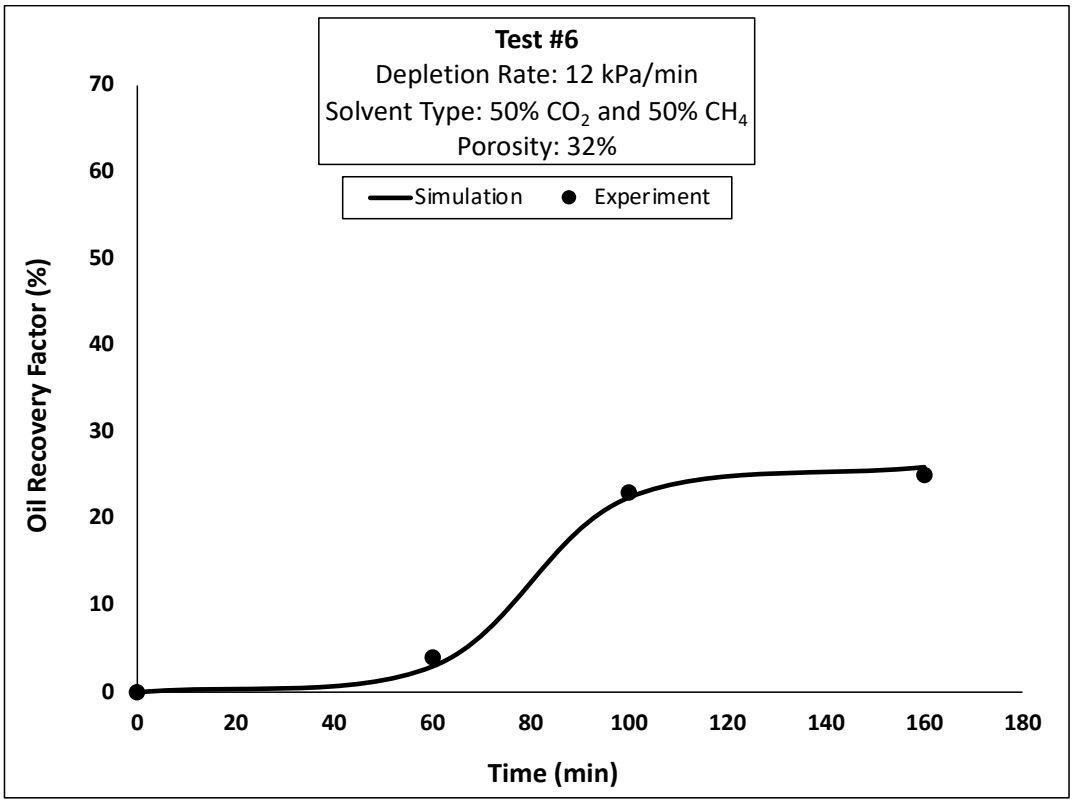

Figure 31. Comparison between the heavy oil recoveries over time for experiment and simulation over time for Test #6.

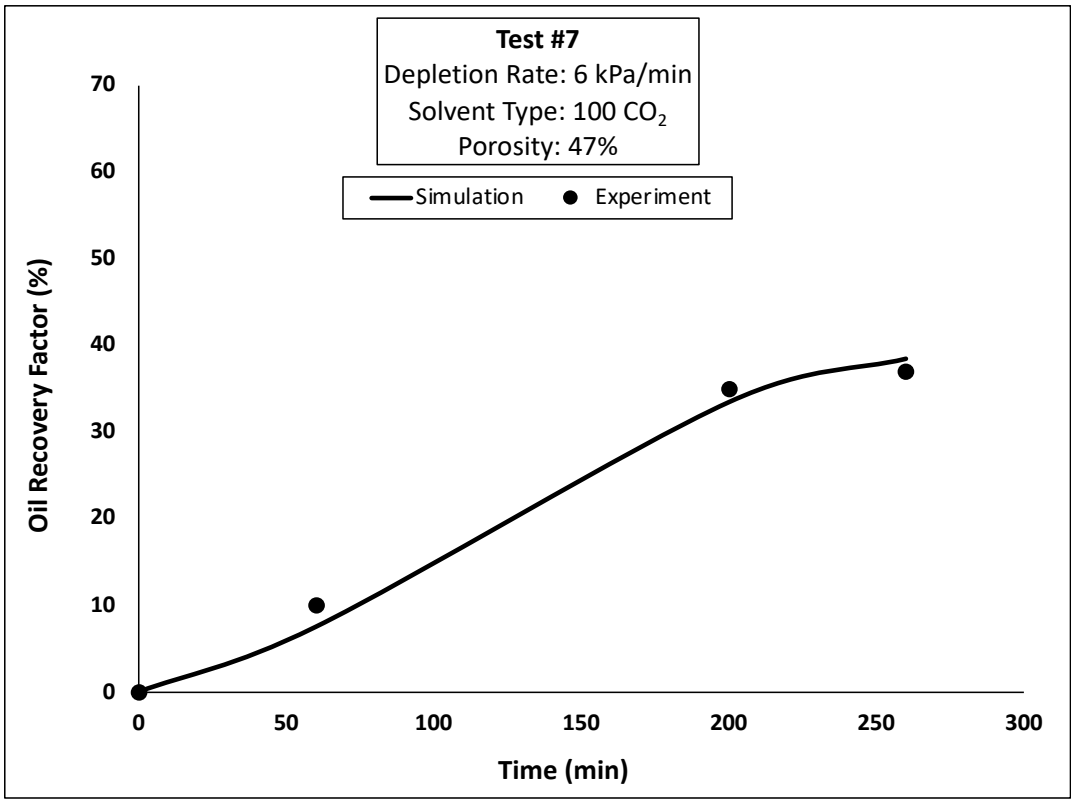

Figure 32. Comparison between the heavy oil recoveries over time for experiment and simulation over time for Test #7.

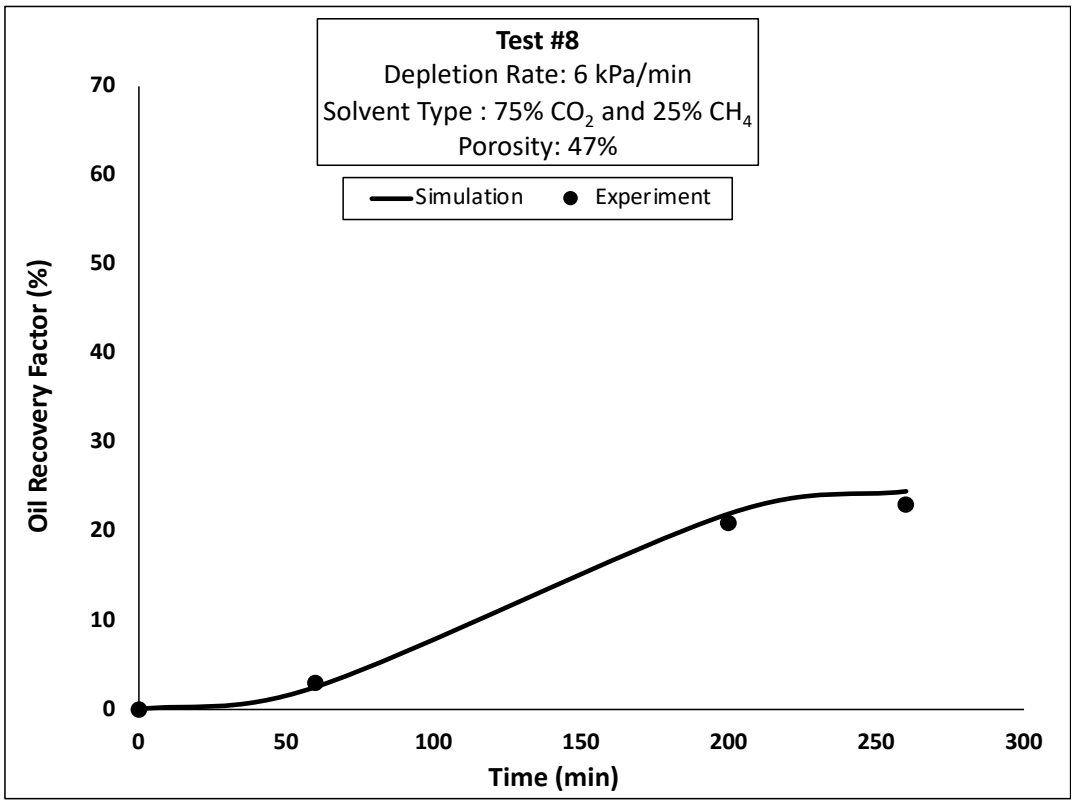

Figure 33. Comparison between the heavy oil recoveries over time for experiment and simulation over time for Test #8.

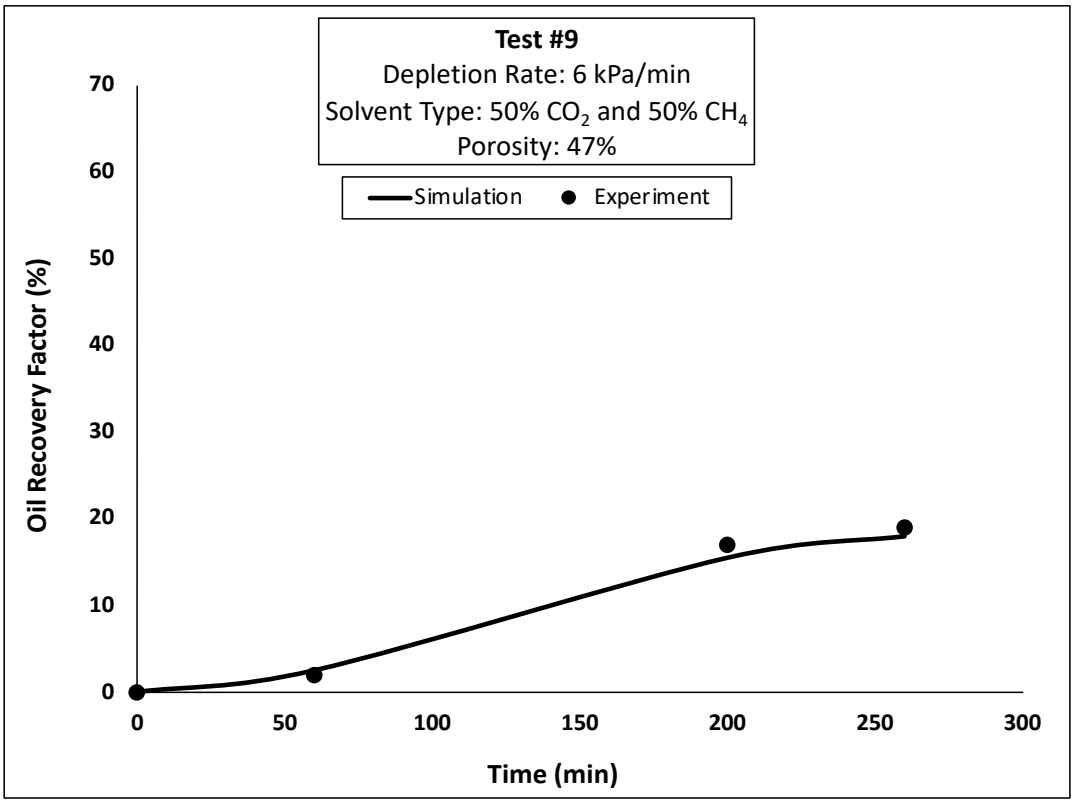

Figure 34. Comparison between the heavy oil recoveries over time for experiment and simulation over time for Test #9.

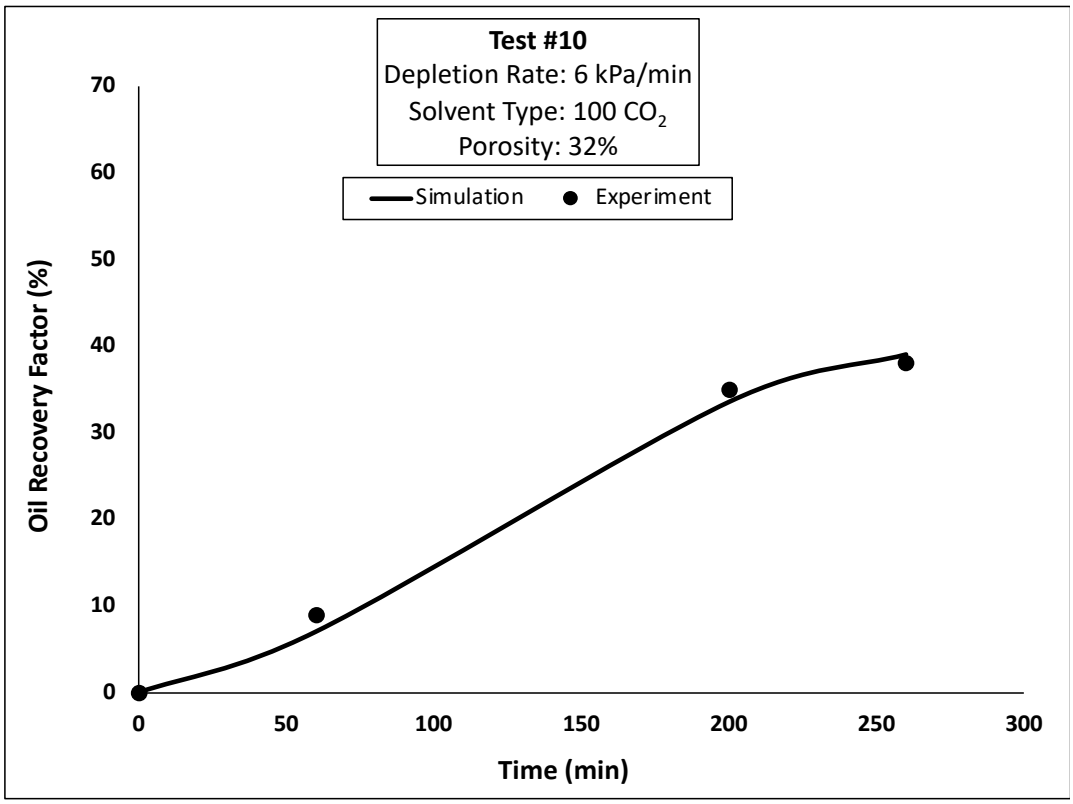

Figure 35. Comparison between the heavy oil recoveries over time for experiment and simulation over time for Test #10.

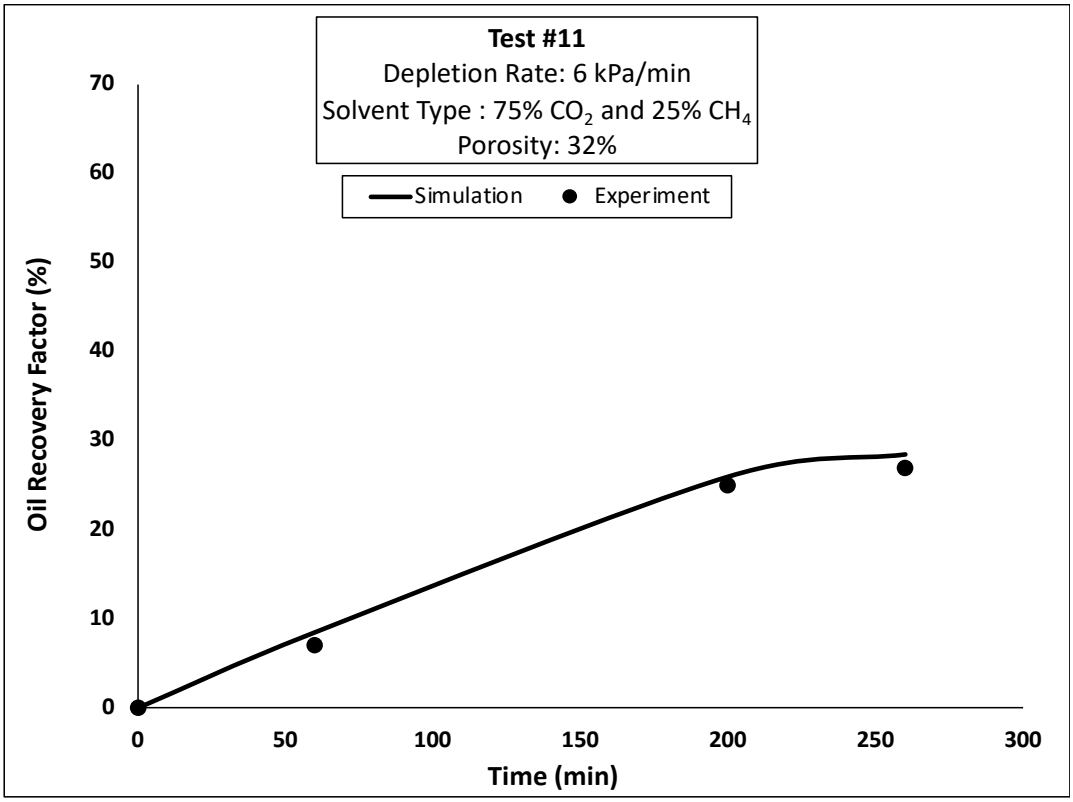

Figure 36. Comparison between the heavy oil recoveries over time for experiment and simulation over time for Test #11.

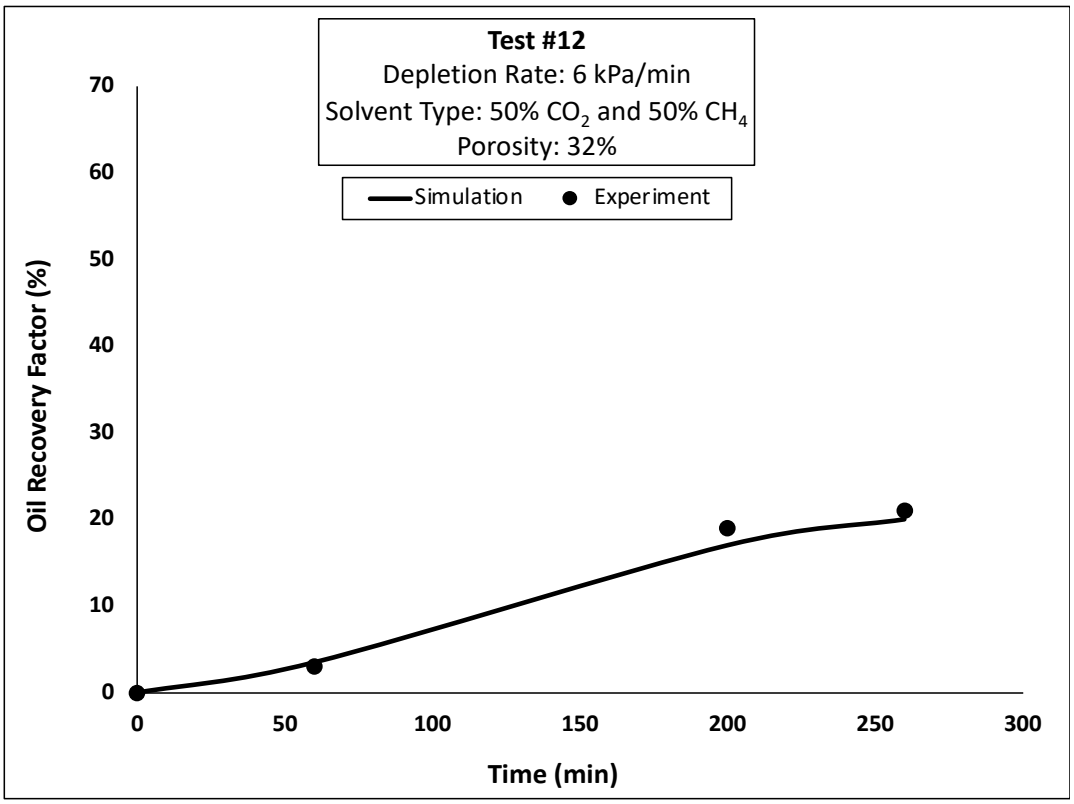

Figure 37. Comparison between the heavy oil recoveries over time for experiment and simulation over time for Test #12.

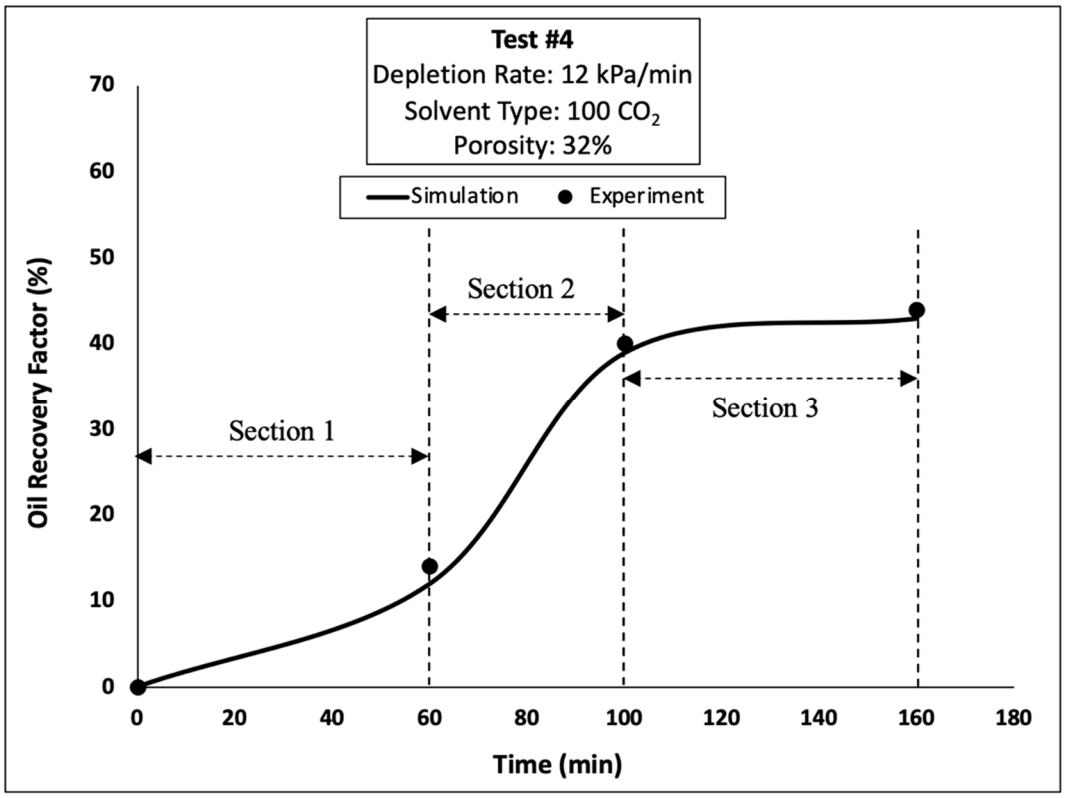

Figure 38. Different stages of pressure depletion for Test #4.

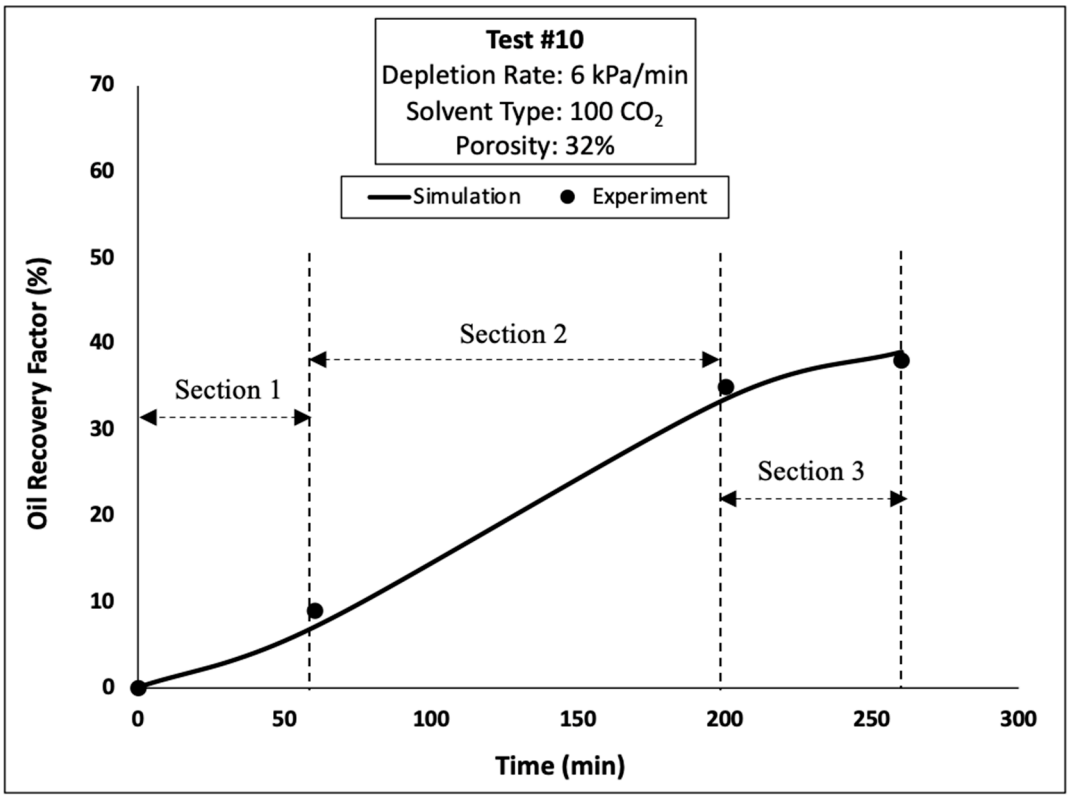

Figure 39. Different stages of pressure depletion for Test #10.

4. Conclusions

This study examined the foamy oil flow dynamics and the overall performance of the CSI process both experimentally and numerically. From the experimental perspective, detailed PVT analysis was performed to assess the physical properties of the heavy oil/solvent systems employed in this project. Moreover, a total of 12 microfluidic CSI tests were performed by employing the reservoir-on-the-chip platforms constructed using a laser machine.

The impact of solvent type on the performance of Cyclic Solvent Injection (CSI) was thoroughly explored by comparing three distinct scenarios. Additionally, meticulous data acquisition methodologies in conjunction with robust image analysis techniques have been conducted to evaluate the overall effectiveness of the CSI process across a variety of reservoir and operational settings. Based on the results of the analysis, solvents containing a higher CO_2 content exhibited superior performance over other solvent compositions. Accordingly, 17% increase in oil recovery was achieved through utilizing 100% CO_2 as solvent compared to utilizing 50% CO_2 and 50% CH_4. A number of mechanisms can be attributed to this observation. Firstly, CO_2 exhibits exceptional capabilities in reducing viscosity and enhancing swelling, as demonstrated through PVT analysis. These dual mechanisms act as driving forces, thereby increasing heavy oil recovery. Furthermore, CO_2 has a higher solubility, ensuring that more gas molecules will be present in scenarios where CO_2 constitutes a greater proportion of the solvent mixture.

The pressure depletion rate is another important factor that influences the foamy oil flow behaviour and the overall performance of the CSI process. According to experiments, a higher depletion rate significantly prolongs foamy oil flow. There are two primary reasons for this phenomenon. A high pressure-depletion rate amplifies the driving force for the nucleation of bubbles. Moreover, it reduces the amount of time available for bubble coalescence. Comparative images depicting varying pressure conditions demonstrated that in the presence of slower depletion rates, portions of dispersed gas tend to coalesce, whereas higher depletion rates maintain separation, resulting in improved quality of foamy oils. A 6% increase in oil recovery was achieved through fast pressure depletion rate compared to slow pressure rate. These discrepancies in recovery outcomes highlight the crucial role played by pressure-depletion rates in shaping the dynamics of foamy oil flow and, thereby, affecting overall recovery efficiency. The insights gained from such analyses can be utilised to optimise CSI processes and unlock the full potential of heavy oil reservoirs by manipulating pressure depletion rates.

Additionally, it was found that a lower reservoir porosity impedes bubble movement and delays coalescence during foamy oil flow. A comparative experiment indicated that lower porosity resulted in superior foamy oil quality as compared to higher porosity. In addition to porosity, permeability of the reservoir also plays an important role in shaping the performance of the process. The higher the permeability of the reservoir, the greater the overall fluid mobility within the reservoir, thereby affecting the recovery factor and efficiency. The intricate interplay between porosity and permeability underscores the multifaceted nature of reservoir dynamics and their profound implications for oil recovery processes.

The CSI process has also been thoroughly investigated from a numerical perspective in this project. First, a PVT model using CMG WINPROP (2021.10) has been history matched and tuned using the experimental PVT results. Moreover, Using the CMG STARS (2021.10), a simulation model was designed to replicate microfluidic CSI tests. As for the simulator calibration, the gas–oil relative permeability, diffusion coefficient, and kinetic model parameters were adjusted to align with the experimental results. The numerical model constructed was found to be accurate in tuning heavy oil recoveries with an average relative error of 7.7%.

Author Contributions: Conceptualization, A.C.; methodology, A.C., M.S. and F.T.; software, A.C.; validation, A.C. and M.S.; formal analysis, F.T.; writing—original draft preparation, A.C.; writing—review and editing, A.C. and F.T.; supervision, F.T. All authors have read and agreed to the published version of the manuscript.

Funding: This research was funded by Petroleum Technology Research Centre (PTRC), grant number HO-UR-04-2021.

Data Availability Statement: The data supporting the findings of this study are available upon request from the corresponding author.

Conflicts of Interest: The authors have no conflicts of interest to declare.

References

1. Smith, G.E. Fluid flow and sand production in heavy-oil reservoirs under solution-gas drive. *SPE Prod. Eng.* **1988**, *3*, 169–180. [CrossRef]
2. Smith, G. Waterflooding heavy oils. In Proceedings of the SPE Rocky Mountain Petroleum Technology Conference/Low-Permeability Reservoirs Symposium, Denver, CO, USA, 18–19 May 1992; p. SPE-24367-MS.
3. Brice, B.W.; Renouf, G. Increasing oil recovery from heavy oil waterfloods. In Proceedings of the SPE International Thermal Operations and Heavy Oil Symposium, Calgary, AB, Canada, 20–23 October 2008; p. SPE-117327-MS.
4. Kovscek, A.R.; Castanier, L.M.; Gerritsen, M.G. Improved predictability of in-situ-combustion enhanced oil recovery. *SPE Reserv. Eval. Eng.* **2013**, *16*, 172–182. [CrossRef]
5. Moore, R.; Laureshen, C.; Mehta, S.; Ursenbach, M.; Belgrave, J.; Weissman, J.; Kessler, R. A downhole catalytic upgrading process for heavy oil using in situ combustion. *J. Can. Pet. Technol.* **1999**, *38*, PETSOC-99-13-44. [CrossRef]
6. Butler, R.M. Steam-assisted gravity drainage: Concept, development, performance and future. *J. Can. Pet. Technol.* **1994**, *33*, 44–50. [CrossRef]
7. Al-Qabandi, S.; Al-Shatti, Y.; Gopalakrishnan, P. Commercial heavy oil recovery by cyclic steam stimulation in Kuwait. In Proceedings of the SPE International Thermal Operations and Heavy Oil Symposium, Calgary, AB, Canada, 19–21 June 1995; p. SPE-30288-MS.
8. White, P.D. In-situ combustion appraisal and status. *J. Pet. Technol.* **1985**, *37*, 1943–1949. [CrossRef]
9. Ali, S.F. CSS-Canada's super strategy for oil sands. *J. Can. Pet. Technol.* **1994**, *33*, PETSOC-94-09-01. [CrossRef] [PubMed]
10. Sabeti, M.; Cheperli, A.; Rahimbakhsh, A.; Torabi, F. A new analytical model to predict heavy oil production rate in the SAGD process. *Can. J. Chem. Eng.* **2023**, *101*, 1648–1659. [CrossRef]
11. Karmaker, K.; Maini, B.B. Applicability of vapor extraction process to problematic viscous oil reservoirs. In Proceedings of the SPE Annual Technical Conference and Exhibition, Denver, CO, USA, 5–8 October 2003; p. SPE-84034-MS.
12. Rahnema, H.; Mamora, D. Combustion assisted gravity drainage (CAGD) appears promising. In Proceedings of the SPE Canada Unconventional Resources Conference, Calgary, AB, Canada, 19–21 October 2010; p. SPE-135821-MS.
13. Luhning, R.; Das, S.; Fisher, L.; Bakker, J.; Grabowski, J.; Engleman, J.; Wong, S.; Sullivan, L.; Boyle, H. Full scale VAPEX process-climate change advantage and economic consequences A. *J. Can. Pet. Technol.* **2003**, *42*, PETSOC-03-02-02. [CrossRef]
14. Das, S.K.; Butler, R.M. Mechanism of the vapor extraction process for heavy oil and bitumen. *J. Pet. Sci. Eng.* **1998**, *21*, 43–59. [CrossRef]
15. Cheperli, A.; Torabi, F.; Sabeti, M.; Rahimbakhsh, A. An Exponential Solvent Chamber Geometry for Modeling the VAPEX Process. *Energies* **2022**, *15*, 5874. [CrossRef]
16. James, L.; Rezaei, N.; Chatzis, I. VAPEX, warm VAPEX and hybrid VAPEX-The state of enhanced oil recovery for in situ heavy oils in Canada. *J. Can. Pet. Technol.* **2008**, *47*, PETSOC-08-04-12-TB. [CrossRef]
17. Ahadi, A.; Torabi, F. Insight into heavy oil recovery of cyclic solvent injection (CSI) utilizing C_3H_8/CH_4 and $C_3H_8/CH_4/CO_2$. *Petroleum* **2018**, *4*, 337–346. [CrossRef]
18. Wang, H.; Torabi, F.; Zeng, F.; Xiao, H. A novel visualization approach for foamy oil non-equilibrium phase behavior study of solvent/live heavy oil systems. *Fuel* **2020**, *272*, 117648. [CrossRef]
19. Lim, G.; Kry, R.; Harker, B.; Jha, C.K. Cyclic stimulation of Cold Lake oil sand with supercritical ethane. In Proceedings of the SPE International Thermal Operations and Heavy Oil Symposium, Calgary, AB, Canada, 19–21 June 1995; p. SPE-30298-MS.
20. Qazvini Firouz, A.; Torabi, F. Feasibility study of solvent-based huff-n-puff method (cyclic solvent injection) to enhance heavy oil recovery. In Proceedings of the SPE Canada Heavy Oil Conference, Calgary, AB, Canada, 12–14 June 2012; p. SPE-157853-MS.
21. Alshmakhy, A.; Maini, B. A follow-up recovery method after cold heavy oil production cyclic CO_2 injection. In Proceedings of the SPE Canada Heavy Oil Conference, Calgary, AB, Canada, 12–14 June 2012; p. SPE-157823-MS.
22. Jia, X.; Zeng, F.; Gu, Y. Pressure pulsing cyclic solvent injection (PP-CSI): A new way to enhance the recovery of heavy oil through solvent-based enhanced oil recovery techniques. In Proceedings of the SPE Annual Technical Conference and Exhibition, New Orleans, LA, USA, 30 September–2 October 2013; p. D021S030R007.
23. Du, Z.; Zeng, F.; Chan, C. An experimental study of the post-CHOPS cyclic solvent injection process. *J. Energy Resour. Technol.* **2015**, *137*, 042901. [CrossRef]

24. Ravel, F.; Anterion, F. Numerical simulation of CO2-heavy oil interactions in fractured medium: An interfacial film concept. In Proceedings of the SPE Annual Technical Conference and Exhibition, Las Vegas, NV, USA, 22–26 September 1985; p. SPE-14228-MS.
25. Ivory, J.; Chang, J.; Coates, R.; Forshner, K. Investigation of cyclic solvent injection process for heavy oil recovery. *J. Can. Pet. Technol.* **2010**, *49*, 22–33. [CrossRef]
26. Chang, J.; Ivory, J. Field-scale simulation of cyclic solvent injection (CSI). *J. Can. Pet. Technol.* **2013**, *52*, 251–265. [CrossRef]
27. Shokri, A.R.; Babadagli, T. Field scale modeling of CHOPS and solvent/thermal based post CHOPS EOR applications considering non-equilibrium foamy oil behavior and realistic representation of wormholes. *J. Pet. Sci. Eng.* **2016**, *137*, 144–156. [CrossRef]
28. Rahimbakhsh, A. Effects of High Permeability Channel Parameters on VAPEX Performance: A Numerical and Experimental Approach Utilizing the Reservoir-on-the-Chip. Ph.D. Dissertation, University of Regina, Regina, SK, Canada, 2023.
29. Peng, D.-Y.; Robinson, D.B. A new two-constant equation of state. *Ind. Eng. Chem. Fundam.* **1976**, *15*, 59–64. [CrossRef]
30. Zhou, X.; Zeng, F.; Zhang, L.; Jiang, Q.; Yuan, Q.; Wang, J.; Zhu, G.; Huang, X. Experimental and mathematical modeling studies on foamy oil stability using a heavy oil–CO_2 system under reservoir conditions. *Fuel* **2020**, *264*, 116771. [CrossRef]
31. Twu, C.H. An internally consistent correlation for predicting the critical properties and molecular weights of petroleum and coal-tar liquids. *Fluid Phase Equilibria* **1984**, *16*, 137–150. [CrossRef]
32. Lee, B.I.; Kesler, M.G. A generalized thermodynamic correlation based on three-parameter corresponding states. *AIChE J.* **1975**, *21*, 510–527. [CrossRef]
33. Pedersen, K.S.; Fredenslund, A. An improved corresponding states model for the prediction of oil and gas viscosities and thermal conductivities. *Chem. Eng. Sci.* **1987**, *42*, 182–186. [CrossRef]
34. Chen, T.; Leung, J.Y.; Bryan, J.L.; Kantzas, A. Analysis of non-equilibrium foamy oil flow in cyclic solvent injection processes. *J. Pet. Sci. Eng.* **2020**, *195*, 107857. [CrossRef]

Disclaimer/Publisher's Note: The statements, opinions and data contained in all publications are solely those of the individual author(s) and contributor(s) and not of MDPI and/or the editor(s). MDPI and/or the editor(s) disclaim responsibility for any injury to people or property resulting from any ideas, methods, instructions or products referred to in the content.